

Movable-Antenna Empowered AAV-Enabled Data Collection over Low-Altitude Wireless Networks

Xuhui Zhang, Wenchao Liu, Jinke Ren, Chunjie Wang, Huijun Xing, Yanyan Shen, and Shuguang Cui

Abstract—Movable-antennas (MAs) are revolutionizing spatial signal processing by providing flexible beamforming in next-generation wireless systems. This paper investigates an MA-empowered autonomous aerial vehicle (AAV) system in low-altitude wireless networks (LAWNs) for uplink data collection from ground users. We aim to maximize the sum achievable rate by jointly optimizing the AAV trajectory, receive beamforming, and MA positions. An efficient alternating optimization (AO) algorithm that incorporates successive convex approximation, weighted minimum mean square error, and particle swarm optimization is developed. The analysis of the computational complexity and convergence features is provided. Extensive simulations demonstrate superior performance in terms of the sum achievable rate and the service reliability comparing to several benchmark schemes. These results demonstrate the distinctive advantages of the proposed scheme: enhanced spectral efficiency via adaptive beam-user alignment and improved collection reliability through spatial interference management, highlighting the implementation potential of the MA-empowered LAWNs.

Index Terms—Low-altitude wireless networks (LAWNs), autonomous aerial vehicles (AAVs), movable-antenna, beamforming design, trajectory design.

I. INTRODUCTION

THE burgeoning low-altitude wireless networks (LAWNs) have emerged as a pivotal enabler for supporting low-altitude economy (LAE) applications, unlocking transformative potential in applications such as emergency logistics, environmental monitoring, and infrastructure inspection [1], [2]. Autonomous aerial vehicles (AAVs), also known as unmanned aerial vehicles (UAVs), as the key aerial devices in the LAWNs, provide dynamic coverage extension, on-demand service deployment, and adaptive resource allocation, thanks to their high mobility and maneuverability [3]. These capabilities allow AAVs to bridge connectivity gaps in remote areas and

enhance situational awareness for time-critical missions [4], [5]. However, the escalating demand for spectrum-intensive tasks, such as high-resolution sensing, latency-sensitive monitoring, and ultra-reliable communications, exacerbates the scarcity of communication resources. Existing single-antenna AAV systems, constrained by limited spatial multiplexing and interference management, fail to meet the throughput requirements of next-generation LAE systems.

Multi-antenna technologies, particularly antenna beamforming, offer a paradigm shift in the AAV-enabled LAWNs by enabling spatial multiplexing, interference suppression, and enhanced spectral efficiency [6]. AAVs equipped with multiple antennas can dynamically adjust radiation patterns to focus energy toward target users, significantly improving signal-to-interference-plus-noise ratio (SINR) and throughput [7]. This capability is critical for supporting dense Internet of things (IoT) deployments and mobile ground users in the LAE scenarios [8]. However, in the AAV-enabled LAWNs, the inherent randomness of user mobility and channel dynamics introduces rapid channel variations and spatially non-stationary interference, resulting in inefficient communication resource utilization. Existing beamforming techniques, designed primarily for static or predictable environments, struggle to maintain precise beam alignment under such dynamic conditions, leading to suboptimal resource utilization and degraded quality of service (QoS) [9].

Movable-antennas (MAs), also referred to fluid antennas [10], further revolutionize the AAV-enabled communication systems by enabling dynamic beam reconfiguration with spatial antenna gains [11], [12]. Unlike fixed-position antennas (FPAs), the MAs allow real-time adjustment of radiation patterns to adapt to user mobility and channel dynamics, thereby enhancing interference mitigation and energy efficiency [13], [14]. When integrated with the AAVs, the MAs unlock synergistic benefits, namely, the aerial mobility of the AAVs complements the beam agility of the MAs, enabling precise alignment with distributed ground users and IoT devices [15]. This hybrid mobility ensures robust connectivity in rapidly changing environments while maintaining low latency and high throughput. Moreover, the AAVs equipped with MAs can exploit spatial-temporal correlations in channel states, optimizing spectrum utilization beyond conventional multi-antenna architectures.

Inspired by the beamforming gains of the MAs, we investigate an AAV-enabled LAWN empowered by the MAs. Meanwhile, the rapid evolution of generative artificial intelligence (GAI) has spurred unprecedented demands for centralized data processing, as massive distributed users require reliable uplink

Xuhui Zhang and Jinke Ren are with the Shenzhen Future Network of Intelligence Institute, the School of Science and Engineering, and the Guangdong Provincial Key Laboratory of Future Networks of Intelligence, The Chinese University of Hong Kong, Shenzhen, Guangdong 518172, China (e-mail: xu.hui.zhang@foxmail.com; jinkeren@cuhk.edu.cn).

Wenchao Liu is with the School of Automation and Intelligent Manufacturing, Southern University of Science and Technology, Shenzhen 518055, China (e-mail: wc.liu@foxmail.com).

Huijun Xing is with the Department of Electrical and Electronic Engineering, Imperial College London, London SW7 2AZ, The United Kingdom (e-mail: huijunxing@link.cuhk.edu.cn).

Chunjie Wang and Yanyan Shen are with Shenzhen Institutes of Advanced Technology, Chinese Academy of Sciences, Guangdong 518055, China (e-mail: cj.wang@siat.ac.cn; yy.shen@siat.ac.cn).

Shuguang Cui is with the School of Science and Engineering, the Shenzhen Future Network of Intelligence Institute, and the Guangdong Provincial Key Laboratory of Future Networks of Intelligence, The Chinese University of Hong Kong, Shenzhen, Guangdong 518172, China (e-mail: shuguangcui@cuhk.edu.cn).

transmission to support latency-sensitive applications. Unlike prior studies focusing on the downlink transmission scenarios, we address the critical yet underexplored challenge of uplink transmission and aim to maximize the data collection rate of ground users in the AAV-enabled LAWN, ensuring efficient spectrum utilization under dynamic channel conditions. The key contributions of this paper are summarized as follows:

- We study a novel MA-empowered uplink communication over the LAWNs, where an AAV is dispatched to collect data from ground users. We formulate an optimization problem to maximize the sum achievable rate of all ground users by jointly optimizing the AAV trajectory, the receive beamforming, the user transmit power, and the antenna positions of the MAs.
- To solve the non-convex problem, we decouple the problem into three sub-problems. Under the alternating optimization (AO) manner, we develop an efficient scheme to optimize the three sub-problems iteratively. The computational complexity and convergence behavior of the proposed scheme are also analyzed.
- We conduct extensive simulations to compare the performance of the proposed scheme with several benchmark schemes. The results demonstrate consistent superiority in sum achievable rate across diverse metrics, validating the efficacy of our proposed scheme.

Organizations: The remainder of this paper is organized as follows. Section II surveys the related works. Section III presents the MA-empowered AAV data collection system for the LAWNs and formulates the sum-rate maximization problem. The AO-based algorithm is developed in Section IV, with complexity and convergence analyses. Performance evaluation is conducted in Section V, followed by concluding remarks in Section VI.

Notations: The following notations are adopted in this work. Let j satisfy $j^2 = -1$ as the imaginary unit. For complex z , $\Re z$ denotes its real part. $\mathbb{C}^{M \times N}$ represents the space of $M \times N$ complex matrices. For matrix \mathbf{G} , \mathbf{G}^H and \mathbf{G}^T denote conjugate transpose and transpose, respectively. For vector \mathbf{w} , $|\mathbf{w}|$ is the Euclidean norm, and $\text{diag}(\mathbf{w})$ constructs a diagonal matrix from \mathbf{w} . $\mathcal{CN}(\mu, \sigma^2)$ indicates a circularly symmetric complex Gaussian distribution with mean μ and variance σ^2 .

II. RELATED WORKS

In this section, we review the existing literature across three interconnected research areas: the AAV-enabled LAWNs, the AAV-enabled data collection systems, and the MA-empowered AAV communications. This structured review establishes the technological landscape motivating our integrated approach. To facilitate reading, a comparison between our work and related works is presented in Table I.

A. AAV-Enabled LAWNs

AAVs have emerged as pivotal elements in the next-generation wireless networks, primarily due to their unique capabilities in on-demand deployment and line-of-sight (LoS) connectivity. Early works [16], [17] established AAVs as aerial

base stations (BSs) for coverage extension in terrestrial networks, demonstrating significant gains in edge-user capacity during temporary events. Meanwhile, several works [18], [19] investigated the AAV-supported relay systems, overcoming terrestrial propagation barriers by establishing dynamic LoS links, thereby enhancing coverage reliability in obstructed environments while minimizing multi-hop latency. Notably, by exploiting the maneuverability inherent to AAVs, optimized trajectory control can provide dynamic adaptation to spatial channel variations to further enhance signal receiving, and energy-efficient coverage provisioning through altitude-dependent path loss minimization [20], [21]. Several works also studied the AAV-enabled LAWNs with integrated sensing and communication (ISAC) [22], [23], localization [24], non-terrestrial networks [25]–[27], and secure communications [28], [29], to provide heterogeneous services for different users. While substantial efforts have focused on downlink-oriented applications, e.g., coverage extension and content relay delivery, the burgeoning data explosion from ground users and IoT devices necessitates rethinking AAV deployment for uplink-dominated applications, particularly in latency-sensitive industrial monitoring and large-scale sensing scenarios.

B. AAV-Enabled Data Collection

Building upon uplink-centric transmission requirements, the AAV-enabled data collection has emerged as a key solution for next-generation wireless networks [30], [31]. Its aerial mobility enables strong LoS-link-enabled data harvesting from ground users with lower energy consumption than the static BSs [32], [33]. Supported by wireless charging stations, the AAV can establish seamless coverage for data collection services to enhance system throughput [34]. Accordingly, the AAV-enabled mobile edge computing (MEC) systems fully utilize the uplink transmission capability for data offloading to the MEC server co-located with the AAVs, or relayed by them [35], [36]. Meanwhile, AAV-enabled over-the-air computation enables simultaneous analog aggregation of collected data through coherent signal superposition, achieving lower latency and energy consumption than conventional digital data aggregation [37], [38]. Besides, through uplink transmission, federated learning can be trained by the AAV-enabled systems, where the AAVs collect the local trained models from ground users, and then aggregate the global model [39]–[41]. While AAV-enabled wireless transmission enhances communication rates to some extent, many existing works adopt fixed single-antenna AAVs. This approach inherently lacks multi-antenna beamforming capabilities for throughput improvement, and the static antenna arrangement fundamentally constrains communication performance.

C. MA-Empowered AAV Communications

Embedding the MAs onto AAV platforms creates a mutually augmented architecture, i.e., the AAV mobility expands positioning flexibility, while the MA reconfigurability enables user-oriented flexible beamforming, jointly unlocking precision beam alignment unattainable in conventional systems. Notably, emerging works demonstrated that the MA-empowered AAV systems achieve substantial improvements

TABLE I: Comparison of Selected Related Works

Ref.	Scenario	Objective	Optimization variables	AAV mobility	MAs	Data collection
[16]	AAV-Enabled LAWNs	Maximizing the long-term rewards	User selection, power level, and subchannel selection	No	No	No
[17]	AAV-enabled LAWNs	Maximizing the temporal average coverage scores	AAV flying direction and distance	Yes	No	No
[18]	AAV-enabled LAWNs	Maximizing the minimum average secrecy rate	AAV trajectory and time scheduling	Yes	No	No
[19]	AAV-enabled LAWNs	Minimizing the total decoding error rate	AAV trajectory, RIS phase shifts, and latency	Yes	No	No
[22]	AAV-enabled ISAC system	Maximizing the weighted sum-rate	AAV maneuver and transmit beamforming	Yes	No	No
[24]	AAV-enabled LAWNs	Maximizing the sum communication rate	AAV deployment, bandwidth and power allocation	Yes	No	No
[26]	AAV-non-terrestrial networks	Maximizing the system utility	Price decision and bandwidth allocation	No	No	No
[28]	AAV-enabled secure systems	Maximizing the achievable transmission rate	Transmit power and jamming power	No	No	No
[31]	AAV-enabled data collection	Minimizing the average age of information	AAVs' beamforming, users' access control, and trajectory planning strategies	Yes	No	Yes
[33]	AAV-enabled data collection	Minimizing the average age of information	AAV trajectory, collection scheduling, and completion time	Yes	No	Yes
[35]	AAV-enabled data collection	Minimizing the weighted sum of the service delay and AAV energy consumption	AAV position, communication and computing resource allocation, and task splitting decisions	Yes	No	Yes
[37]	AAV-enabled data collection	Maximizing the minimum amount of tasks	AAV trajectory, transceiver design, cluster scheduling and association	Yes	No	Yes
[38]	AAV-enabled data collection	Minimizing the mean square error	AAV deployment and precoding coefficients of sensors	Yes	No	Yes
[41]	AAV-enabled data collection	Minimizing the latency	AAV trajectory, bandwidth allocation, computing resources, and transmit power	Yes	No	Yes
[42]	MA-AAV communications	Maximizing the achievable data rate	AAV trajectory, transmit beamforming, and the positions of the MA	Yes	Yes	No
[43]	MA-AAV communications	Maximizing the SINR	Antenna position vector, array rotation vector, receive beamforming vector, and associated BS of the AAV	No	Yes	No
Our work	MA-empowered AAV-enabled data collection	Maximizing the sum-rate of users	AAV trajectory, receive beamforming, MA position, and user transmit power	Yes	Yes	Yes

in both communication throughput and interference mitigation capabilities. Specifically, in [42], an MA-empowered AAV-enabled downlink transmission system was considered, and the achievable data rate was maximized by optimizing the antenna position, beamforming, and AAV trajectory. Moreover, a six-dimensional MA array was adopted in [43] to enhance the interference mitigation for the AAV communication systems. Consequently, we are motivated to investigate user-centric uplink transmission in AAV-enabled data collection systems, where the synergistic integration of the MA mobility, the receive beamforming, and the AAV trajectory design achieves data collection rate enhancement for the collection tasks.

III. SYSTEM MODEL AND PROBLEM FORMULATION

A. System Model

As shown in Fig. 1, an MA-enabled uplink communication system is considered, where an AAV is dispatched to fly over a designated region and collect data from M ground users. Each user is equipped with a single FPA, and the set of users is denoted as $\mathcal{M} \triangleq \{1, 2, \dots, M\}$. The AAV is equipped with K receive MAs, whose position can be flexibly adjusted within a given two-dimensional plane.¹ All users share the same bandwidth on the uplink transmission to send data to the AAV, while also considering the mutual interference between users. The system operates within a designated mission period T , which is divided into N time slots, each with a duration

¹Noting that we assume that all antennas are placed vertically to the horizontal plane [44]. Without loss of generality, we consider that the AAV's flight direction is independent of the vertical and horizontal angle-of-arrival (AoA) of the radiated communication signal beams, thereby simplifying the design of the MA position.

of $\tau = \frac{T}{N}$, and the set of the time slots is denoted as $\mathcal{N} \triangleq \{1, \dots, N\}$.

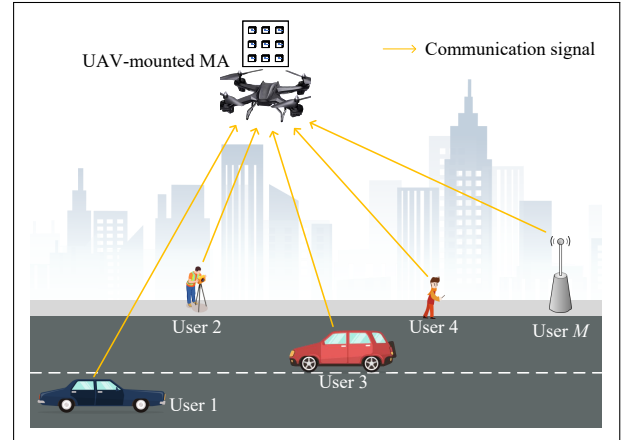


Fig. 1: The system model.

A three-dimensional Cartesian coordinate system is utilized to represent the position of the AAV and the users, where the location of the m -th user is denoted by $\mathcal{P}_m = [s_m, 0]$, where $s_m = [x_m, y_m]$ represents the horizontal coordinates. The AAV flies at a fixed altitude H , which is sufficiently high to avoid any obstacles including terrains, towers, and buildings. Additionally, given the short duration of each time slot, the AAV can be regarded as quasi-static within each time slot. Consequently, the position of the AAV at time slot n is denoted as $\mathbf{Q}_n = [\mathbf{q}_n, H]$, where $\mathbf{q}_n = [x_n, y_n]$ is the horizontal coordinates. The AAV departs from the starting position \mathbf{q}_1 at the beginning of each mission period, and returns to the

end position \mathbf{q}_F at the end of each mission period. During the entire flight, the AAV complies with the mobility constraints, with the maximum velocity V_{\max} and maximum acceleration a_{\max} . Thus, the mobility constraints can be given by

$$\mathbf{q}_1 = \mathbf{q}_I, \quad \mathbf{q}_N = \mathbf{q}_F, \quad (1)$$

$$\|\mathbf{v}_n\| = \frac{\|\mathbf{q}_n - \mathbf{q}_{n-1}\|}{\tau} \leq V_{\max}, \quad \forall n \in \mathcal{N} \setminus \{1\}, \quad (2)$$

$$\|\mathbf{a}_n\| = \frac{\|\mathbf{v}_n - \mathbf{v}_{n-1}\|}{\tau} \leq a_{\max}, \quad \forall n \in \mathcal{N} \setminus \{1, 2\}. \quad (3)$$

We consider that the channel among the AAV and the users depends not only on the propagation environment but also on the position of the MA. Similarly to [13], [45], we adopt a far field-response based channel model, where the sizes of the MA moving region for the AAV is much smaller than the signal propagation distance. Then, the angle-of-departure (AoD), the AoA, and the complex coefficient amplitude for each channel path between each user and the AAV remain constant regardless of the MA's position within the designated region, while only the phases of the multi-path channels vary.

Let $\mathbf{u}_{k,n} = [x_{k,n}, y_{k,n}] \in \mathcal{R}_s$ denote the position of the k -th MA at the AAV in time slot n , where \mathcal{R}_s is the square region with size $L \times L$ in planes. Then, the position vector of all K MAs is denoted by $\mathbf{u}_n \triangleq [\mathbf{u}_{1,n}, \mathbf{u}_{2,n}, \dots, \mathbf{u}_{K,n}]^T \in \mathbb{R}^{K \times 2}$. To avoid potential electrical coupling between adjacent MAs, which could reduce antenna efficiency, a minimum inter-MA distance d_{\min} is required between each pair of MAs at the AAV, i.e.

$$\|\mathbf{u}_{i,n} - \mathbf{u}_{j,n}\| \geq d_{\min}, \quad \forall i \neq j, \forall i, j \in \mathcal{K}, \forall n \in \mathcal{N}. \quad (4)$$

We assume that the transmission path between the m -th user and the AAV is L_m^t . Then, we can use the $\theta_{m,i,n}$ and $\phi_{m,i,n}$ to represent the vertical AoA and the horizontal AoA of the i -th transmission path. We assume that the AoA of all paths follows a uniform distribution in Δ , which can be expressed as $\theta_{m,i,n} \in (\theta_{m,n} - \Delta/2, \theta_{m,n} + \Delta/2)$, and $\phi_{m,i,n} \in (\phi_{m,n} - \Delta/2, \phi_{m,n} + \Delta/2)$, where $\theta_{m,n}$ and $\phi_{m,n}$ are related with the locations of the m -th user and the AAV, which are given by

$$\theta_{m,n} = \arcsin \frac{H}{d_{m,n}}, \quad (5)$$

$$\varphi_{m,n} = \arccos \frac{y_n - y_m}{\|\mathbf{q}_n - \mathbf{s}_m\|}, \quad (6)$$

where $d_{m,n} = \sqrt{\|\mathbf{q}_n - \mathbf{s}_m\|^2 + H^2}$ represents the distance between the m -th user and the AAV. Then, for the m -th user, the signal propagation phase difference of the i -th transmission path between the k -th MA position $\mathbf{u}_{k,n}$ and original position $\mathbf{u}_0 = [0, 0]^T$ at the AAV can be given by

$$\begin{aligned} \rho_{m,k,i,n} &= x_{k,n} \sin \theta_{m,i,n} \cos \phi_{m,i,n} \\ &\quad + y_{k,n} \sin \theta_{m,i,n} \sin \phi_{m,i,n}. \end{aligned} \quad (7)$$

Therefore, the corresponding receive field response vector (FRV) from the m -th user to the k -th MA at the AAV can be expressed as

$$g_{m,k,n} = \left[e^{j \frac{2\pi}{\lambda} \rho_{m,k,1,n}}, \dots, e^{j \frac{2\pi}{\lambda} \rho_{m,k,L_m^t,n}} \right]^T \in \mathbb{C}^{L_m^t \times 1}, \quad (8)$$

and the receive field response matrix can be represented as

$$\mathbf{G}_{m,n} = [g_{m,1,n}, g_{m,2,n}, \dots, g_{m,K,n}] \in \mathbb{C}^{L_m^t \times K}. \quad (9)$$

Since the user is equipped with single FPA, the transmit FRV for the m -th user is given by

$$\mathbf{f}_m = [1, 1, \dots, 1]^T \in \mathbb{R}^{L_m^t \times 1}. \quad (10)$$

In addition, we define a path response matrix (PRM) $\Sigma_{m,n} = \text{diag}(\sigma_{m,1,n}, \dots, \sigma_{m,L_m^t,n}) \in \mathbb{C}^{L_m^t \times L_m^t}$, where $\sigma_{m,i,n}$ for $i = 1, 2, \dots, L_m^t$ represents the complex amplitude response for the i -th transmission path between the m -th user and the AAV. The complex amplitude response $\sigma_{m,i,n}$ can be expressed as $\sigma_{m,i,n} = \sqrt{\frac{\alpha_{m,n}}{L_m^t}} g_{m,i,n}$, where $\alpha_{m,n}$ denotes the large-scale fading channel gain and $g_{m,i,n}$ denotes the small-scale fading coefficients [46]. The large-scale fading channel gain $\alpha_{m,n}$ can be expressed as $\alpha_{m,n} = h_0 d_{m,n}^{-2}$, where h_0 denotes the channel power gain at a reference distance of 1m [44]. Thus, the channel vector between the m -th user and the AAV can be expressed as

$$\begin{aligned} \mathbf{h}_{m,n} &= \mathbf{G}_{m,n}^H \Sigma_{m,n} \mathbf{f}_m \\ &= [\bar{h}_{m,1,n}, \bar{h}_{m,2,n}, \dots, \bar{h}_{m,K,n}]^T \in \mathbb{C}^{K \times 1}. \end{aligned} \quad (11)$$

where $\bar{h}_{m,k,n} = \sum_{i=1}^{L_m^t} \sigma_{m,i,n} e^{-j \frac{2\pi}{\lambda} \rho_{m,k,i,n}}$.

Hence, the received signal from the m -th user is given by

$$\begin{aligned} \mathbf{z}_{m,n} &= \mathbf{w}_{m,n}^H \left(\sum_{r \in \mathcal{M}} \sqrt{p_{r,n}} \mathbf{h}_{r,n} s_{r,n} + \tilde{\mathbf{n}}_n \right) \\ &= \underbrace{\mathbf{w}_{m,n}^H \sqrt{p_{m,n}} \mathbf{h}_{m,n} s_{m,n}}_{\text{desired signal}} + \underbrace{\sum_{r=1, r \neq m}^M \mathbf{w}_{m,n}^H \sqrt{p_{r,n}} \mathbf{h}_{r,n} s_{r,n}}_{\text{multiuser interference}} \\ &\quad + \mathbf{w}_{m,n}^H \tilde{\mathbf{n}}_n, \end{aligned} \quad (12)$$

where $\mathbf{w}_{m,n}$ denotes the receive beamforming vector of the AAV, $s_{r,n}$ denotes the information symbol for the r -th user which satisfies $\mathbb{E}[|s_{r,n}|^2] = 1$, $p_{r,n}$ denotes the transmit power of the r -th user, $\tilde{\mathbf{n}}_n \in \mathcal{CN}(\mathbf{0}, \sigma_{\text{AAV}}^2 \mathbf{I}_K)$ is the noise vector at the AAV. Thus, the received signal-to-interference-plus-noise ratio (SINR) of the AAV in time slot n is given by

$$\gamma_{m,n} = \frac{p_{m,n} |\mathbf{w}_{m,n}^H \mathbf{h}_{m,n}|^2}{\sum_{r=1, r \neq m}^M p_{r,n} |\mathbf{w}_{m,n}^H \mathbf{h}_{r,n}|^2 + \|\mathbf{w}_{m,n}\|_2^2 \sigma_{\text{AAV}}^2}. \quad (13)$$

Then, the uplink transmission rate for the m -th user can be given by $R_{m,n} = \log_2(1 + \gamma_{m,n})$.

B. Problem Formulation

In this work, we focus on maximizing the sum-rate for all users under receive power constraints. This is accomplished through the joint optimization of the AAV trajectory $\mathbf{Q} \triangleq \{\mathbf{q}_n, \forall n\}$, the receive beamforming $\mathbf{W} \triangleq \{\mathbf{w}_{m,n}, \forall m, \forall n\}$, the MA position $\mathbf{U} \triangleq \{\mathbf{u}_{k,n}, \forall k, \forall n\}$ and the user transmit

power $\mathbf{P} \triangleq \{p_{m,n}, \forall m, \forall n\}^2$. Therefore, the optimization problem can be formulated as

$$(\mathbf{P1}) : \max_{\mathbf{Q}, \mathbf{W}, \mathbf{U}, \mathbf{P}} \sum_{n=1}^N \sum_{m=1}^M R_{m,n} \quad (14a)$$

$$\text{s.t. } \mathbf{q}_1 = \mathbf{q}_I, \quad \mathbf{q}_N = \mathbf{q}_F, \quad (14b)$$

$$\|\mathbf{v}_n\| \leq V_{\max}, \forall n \in \mathcal{N} \setminus \{1\}, \quad (14c)$$

$$\|\mathbf{a}_n\| \leq a_{\max}, \forall n \in \mathcal{N} \setminus \{1, 2\}, \quad (14d)$$

$$\|\mathbf{w}_{m,n}\|^2 \leq 1, \forall m \in \mathcal{M}, \forall n \in \mathcal{N}, \quad (14e)$$

$$\|\mathbf{u}_{i,n} - \mathbf{u}_{j,n}\| \geq d_{\min}, \forall i \neq j, \forall i, j \in \mathcal{K}, \forall n \in \mathcal{N}, \quad (14f)$$

$$\mathbf{u}_{k,n} \in \mathcal{R}_s, \forall k \in \mathcal{K}, \forall n \in \mathcal{N}, \quad (14g)$$

$$0 \leq p_{m,n} \leq P_{\max}, \forall m \in \mathcal{M}, \forall n \in \mathcal{N}, \quad (14h)$$

where constraints (14b)-(14d) represent the AAV kinematic constraints, (14e) represents the feasible region constraint of the receive beamforming, (14f) is the minimum distance constraint between adjacent MAs, (14g) represents the MA mobility constraint, (14h) denotes the transmit power constraint of the users.

Remark 1. Due to the extremely complex form in which the MA position appear in Eqs. (7) and (11) for the channel vectors between the users and the AAV, the uplink transmission rates exhibit a highly non-convex dependency on the MA position. Additionally, when the MA position are fixed, there is a strong coupling between the AAV trajectory and the beamforming variables. Furthermore, the optimization objective of Problem (P1) is non-concave, making the direct search for an optimal solution extremely difficult. Therefore, we propose an AO algorithm based on BCA, which seeks a suboptimal solution by alternately optimizing the beamforming, the AAV trajectory, the MA position, and the user transmit power.

IV. PROPOSED ALTERNATING OPTIMIZATION ALGORITHM

A. AAV Trajectory Optimization

Given feasible receive beamforming \mathbf{W} , MA position \mathbf{U} and user transmit power \mathbf{P} , the subproblem of optimizing the AAV trajectory \mathbf{Q} is formulated as follows

$$(\mathbf{P2}) : \max_{\mathbf{Q}} \sum_{n=1}^N \sum_{m=1}^M R_{m,n} \quad (15a)$$

$$\text{s.t. } (14b) - (14d). \quad (15b)$$

Clearly, the objective function (15a) is non-convex with respect to \mathbf{q} . The variable \mathbf{q} is included in both the received FRV and the PRM, which makes solving the problem (P2) optimally very challenging. To simplify the trajectory design, we use the AAV trajectory from the l -th iteration to approximate the receive FRV $g_{m,k,n}$ in the $(l+1)$ -th iteration [47]. As a result, the approximate receive FRV is given as

$$\tilde{g}_{m,k,n} = \left[e^{j \frac{2\pi}{\lambda} \tilde{\rho}_{m,k,1,n}}, \dots, e^{j \frac{2\pi}{\lambda} \tilde{\rho}_{m,k,L_m^t,n}} \right]^T, \quad (16)$$

²Given that the AAV's flight energy consumption significantly exceeds that of the MA movement and data collection, this work prioritizes enhancing the user data collection performance by optimizing the communication resource allocation and AAV trajectory design. Consequently, the energy consumption regarding the AAV aerodynamics will be addressed in our future works.

where

$$\tilde{\rho}_{m,k,i,n} = x_{k,n} \sin \theta_{m,i,n}^{(l)} \cos \phi_{m,i,n}^{(l)} + y_{k,n} \sin \theta_{m,i,n}^{(l)} \sin \phi_{m,i,n}^{(l)}. \quad (17)$$

Additionally, to ensure the accuracy of this approximation, we introduce a trust region constraint as [22]

$$\|\mathbf{q}_n^{(l)} - \mathbf{q}_n^{(l-1)}\| \leq \phi^l, \forall n \in \mathcal{N}, \quad (18)$$

where ϕ^l denotes the radius of the trust region in the l -th iteration.

Next, we focus only on the part of the PRM that is related to \mathbf{q} , i.e.

$$\begin{aligned} \Sigma_{m,n} &= \text{diag}(\sigma_{m,1,n}, \dots, \sigma_{m,L_m^t,n}) \\ &= \sqrt{\frac{\alpha_{m,n}}{L_m^t}} \text{diag}(g_{m,1,n}, \dots, g_{m,L_m^t,n}) \\ &= \frac{1}{d_{m,n}} \text{diag}\left(\sqrt{\frac{h_0}{L_m^t}} g_{m,1,n}, \dots, \sqrt{\frac{h_0}{L_m^t}} g_{m,L_m^t,n}\right). \end{aligned} \quad (19)$$

Thus, the channel vector from the m -th user to the AAV can be reformulated as

$$\tilde{\mathbf{h}}_{m,n} = \frac{1}{d_{m,n}} \left[\tilde{h}_{m,1,n}, \tilde{h}_{m,2,n}, \dots, \tilde{h}_{m,K,n} \right]^T. \quad (20)$$

where $\tilde{h}_{m,k,n} = \sqrt{\frac{h_0}{L_m^t}} \sum_{i=1}^{L_m^t} g_{m,i,n} e^{-j \frac{2\pi}{\lambda} \tilde{\rho}_{m,k,i,n}}$. For simplicity, we let

$$\mathbf{h}_{m,n}^{\Xi} = \left[\tilde{h}_{m,1,n}, \tilde{h}_{m,2,n}, \dots, \tilde{h}_{m,K,n} \right]^T, \quad (21)$$

and $\tilde{\mathbf{h}}_{m,n} = \frac{1}{d_{m,n}} \mathbf{h}_{m,n}^{\Xi}$. Then, the uplink transmission rate for the m -th user can be reformulated as

$$\begin{aligned} R_{m,n} &= \log_2 \left(1 + \frac{d_{m,n}^{-2} p_{m,n} |\mathbf{w}_{m,n}^H \mathbf{h}_{m,n}^{\Xi}|^2}{\sum_{r=1, r \neq m}^{\mathcal{M}} d_{r,n}^{-2} p_{r,n} |\mathbf{w}_{m,n}^H \mathbf{h}_{r,n}^{\Xi}|^2 + \|\mathbf{w}_{m,n}^H\|_2^2 \sigma_{\text{AAV}}^2} \right) \\ &= \log_2 \left(\sum_{r=1}^{\mathcal{M}} d_{r,n}^{-2} p_{r,n} |\mathbf{w}_{m,n}^H \mathbf{h}_{r,n}^{\Xi}|^2 + \|\mathbf{w}_{m,n}^H\|_2^2 \sigma_{\text{AAV}}^2 \right) \\ &\quad - \log_2 \left(\sum_{r=1, r \neq m}^{\mathcal{M}} d_{r,n}^{-2} p_{r,n} |\mathbf{w}_{m,n}^H \mathbf{h}_{r,n}^{\Xi}|^2 + \|\mathbf{w}_{m,n}^H\|_2^2 \sigma_{\text{AAV}}^2 \right). \end{aligned} \quad (22)$$

Then, the first term of $R_{m,n}$ can be reformulated as

$$\begin{aligned} &\log_2 \left(\sum_{r=1}^{\mathcal{M}} d_{r,n}^{-2} p_{r,n} |\mathbf{w}_{m,n}^H \mathbf{h}_{r,n}^{\Xi}|^2 + \|\mathbf{w}_{m,n}^H\|_2^2 \sigma_{\text{AAV}}^2 \right) \\ &\geq \log_2 \left(\sum_{r=1}^{\mathcal{M}} (d_{r,n}^{(l)})^{-2} p_{r,n} |\mathbf{w}_{m,n}^H \mathbf{h}_{r,n}^{\Xi}|^2 + \|\mathbf{w}_{m,n}^H\|_2^2 \sigma_{\text{AAV}}^2 \right) \\ &\quad + \sum_{r=1}^{\mathcal{M}} E_{r,n} \left((d_{r,n}^{(l)})^2 - d_{r,n}^2 \right) \triangleq \hat{R}_{m,n}^{\text{first}}, \end{aligned}$$

where $d_{r,n}^{(l)} = \sqrt{\|\mathbf{q}_n^{(l)} - \mathbf{s}_r\|^2 + H^2}$ represents the distance between the AAV and the user r in the l -th iteration, and

$$E_{r,n} = \frac{\log_2(e)(d_{r,n}^{(l)})^{-4} \left(\sum_{r=1}^M p_{r,n} |\mathbf{w}_{m,n}^H \mathbf{h}_{r,n}^\Xi|^2 \right)}{\left(\sum_{r=1}^M (d_{r,n}^{(l)})^{-2} p_{r,n} |\mathbf{w}_{m,n}^H \mathbf{h}_{r,n}^\Xi|^2 \right) + \|\mathbf{w}_{m,n}^H\|_2^2 \sigma_{\text{AAV}}^2}. \quad (23)$$

Since $d_{m,n}$ is convex with respect to \mathbf{q} , $\hat{R}_{m,n}^{\text{first}}$ is concave with respect to \mathbf{q} . Moreover, the second term of $R_{m,n}$ is non-convex with respect to \mathbf{q} . To convert it to convex form, we introduce the slack variable $\eta_{m,n}$, which satisfies

$$\frac{1}{e^{\eta_{m,n}}} \leq (d_{m,n}^{(l)})^2 + 2(\mathbf{q}_n^{(l)} - \mathbf{s}_m)^T (\mathbf{q}_n - \mathbf{q}_n^{(l)}), \quad (24)$$

$$\forall m \in \mathcal{M}, \forall n \in \mathcal{N}.$$

Then, the second term of $R_{m,n}$ can be reformulated as

$$\begin{aligned} & \log_2 \left(\sum_{r=1, r \neq m}^M d_{r,n}^{-2} p_{r,n} |\mathbf{w}_{m,n}^H \mathbf{h}_{r,n}^\Xi|^2 + \|\mathbf{w}_{m,n}^H\|_2^2 \sigma_{\text{AAV}}^2 \right) \\ & \leq \log_2 \left(\sum_{r=1, r \neq m}^M e^{\eta_{r,n}} p_{r,n} |\mathbf{w}_{m,n}^H \mathbf{h}_{r,n}^\Xi|^2 + \|\mathbf{w}_{m,n}^H\|_2^2 \sigma_{\text{AAV}}^2 \right) \\ & \triangleq \check{R}_{m,n}^{\text{second}}. \end{aligned} \quad (25)$$

By replacing $R_{m,n}$ as its lower bound $\hat{R}_{m,n}^{\text{first}} - \check{R}_{m,n}^{\text{second}}$, the AAV trajectory optimization problem is approximated as the form below

$$(\mathbf{P2-1}) : \max_{\mathbf{Q}, \eta} \sum_{n=1}^N \sum_{m=1}^M (\hat{R}_{m,n}^{\text{first}} - \check{R}_{m,n}^{\text{second}}) \quad (26a)$$

$$\text{s.t.} \quad (14b) - (14d), (24), \quad (26b)$$

where $\eta = \{\eta_{m,n}, \forall m, \forall n\}$. Problem (P2-1) is a convex optimization problem, which can be efficiently solved by standard convex optimization solvers such as CVX toolbox. The detailed procedure to solve problem (P2-1) is summarized in Algorithm 1.

Algorithm 1 SCA-based Algorithm for Solving P2-1

Input: An initial feasible solution of trajectory \mathbf{Q}^l ;
Initialize: the iteration number $l = 0$;
Initialize: the small precision threshold ϵ ;
Initialize: the maximum number of iterations l_{max} ;
1: **repeat**
2: Solve the problem P2-1, get the solution \mathbf{Q}^l ;
3: Update the values of optimization variables;
4: Compute the objective function \bar{R}^l via (26a);
5: Set $l = l + 1$;
6: **until** $|\bar{R}^l - \bar{R}^{l-1}| < \epsilon$ or $l = l_{\text{max}}$;
Output: \mathbf{Q}^l, \bar{R}^l .

B. Receive Beamforming and User Transmit Power

Given feasible AAV trajectory \mathbf{Q} and the MA position \mathbf{U} , the subproblem of optimizing the receive beamforming \mathbf{W} and the user transmit power \mathbf{P} is formulated as follows

$$(\mathbf{P3}) : \max_{\mathbf{W}, \mathbf{P}} \sum_{n=1}^N \sum_{m=1}^M R_{m,n} \quad (27a)$$

$$\text{s.t.} \quad (14f), (14h). \quad (27b)$$

Problem (P3) poses significant challenges owing to the non-convex nature of the constraints delineated in (27a). Furthermore, there exists a strong coupling between the user transmit power \mathbf{P} and the beamforming \mathbf{W} , which complicates the problem further. To make problem (P3) more tractable, we employ the weighted mean square error (WMMSE) method [48] to equivalently reformulate $R_{m,n}$ in the constraint (27a), as depicted in (28).

This transformation entails the introduction of auxiliary variables $\beta = \{\beta_{m,n}, \forall m, \forall n\}$ and $\omega = \{\omega_{m,n}, \forall m, \forall n\}$. Therefore, the optimization problem is approximated in the following form

$$(\mathbf{P3-1}) : \max_{\mathbf{W}, \mathbf{P}, \beta, \omega} \sum_{n=1}^N \sum_{m=1}^M \tilde{R}_{m,n} \quad (29a)$$

$$\text{s.t.} \quad (14e), (14h), \quad (29b)$$

$$\omega_{m,n} \geq 0, \forall m, \forall n. \quad (29c)$$

Subsequently, we propose to utilize the BCA method to address the problem (P3-1).

1) *Updating Auxiliary Variables:* Based on the derivation of the WMMSE transformation, the auxiliary variables $\{\omega_{m,n}\}$ and $\{\beta_{m,n}\}$ can be updated using the following closed-form solutions, given the other variables:

$$\beta_{m,n}^{\text{opt}} = \frac{\sqrt{p_{m,n}} \mathbf{w}_{m,n}^H \mathbf{h}_{m,n}}{\sum_{r=1}^M p_{r,n} |\mathbf{w}_{m,n}^H \mathbf{h}_{r,n}|^2 + \|\mathbf{w}_{m,n}^H\|_2^2 \sigma_{\text{AAV}}^2}, \quad (30)$$

$$\omega_{m,n}^{\text{opt}} = 1 + \frac{p_{m,n} |\mathbf{w}_{m,n}^H \mathbf{h}_{m,n}|^2}{\sum_{r=1, r \neq m}^M p_{r,n} |\mathbf{w}_{m,n}^H \mathbf{h}_{r,n}|^2 + \|\mathbf{w}_{m,n}^H\|_2^2 \sigma_{\text{AAV}}^2}. \quad (31)$$

2) *Updating Receive Beamforming:*

$$(\mathbf{P3-2}) : \max_{\mathbf{W}} \sum_{n=1}^N \sum_{m=1}^M \tilde{R}_{m,n} \quad (32a)$$

$$\text{s.t.} \quad (14e). \quad (32b)$$

Problem (P3-2) is a convex optimization problem, which can be efficiently solved by standard convex optimization solvers such as CVX. Moreover, by introducing dual variables associated with the constraints (14e), we can derive a Lagrangian dual function and thus a closed optimal solution can be derived. Concrete information is shown in Theorem 1.

Theorem 1. For problem (P3-2), the optimal receive beamforming can be expressed as

$$\begin{aligned} \mathbf{w}_{m,n}^{\text{opt}} = & \frac{\omega_{m,n} \sqrt{p_{m,n}} \mathbf{h}_{m,n} \beta_{m,n}^*}{\omega_{m,n} |\beta_{m,n}|^2 \left(\sum_{r=1}^M p_{r,n} \mathbf{h}_{m,n}^* \mathbf{h}_{r,n} + \sigma_{\text{AAV}}^2 \mathbf{I} \right) + \lambda_{m,n} \mathbf{I}}, \end{aligned} \quad (33)$$

where $\{\lambda_{m,n}\}$ are the dual variables associated with the corresponding constraints (14e).

Proof. Please refer to Appendix A. \square

$$\begin{aligned}
R_{m,n} &= \max_{\omega_{m,n} \geq 0} \log_2(\omega_{m,n}) - \omega_{m,n} \left(\sum_{r=1}^{\mathcal{M}} p_{r,n} \left| \mathbf{w}_{m,n}^H \mathbf{h}_{r,n} \right|^2 + \|\mathbf{w}_{m,n}^H\|_2^2 \sigma_{\text{AAV}}^2 \right)^{-1} \sqrt{p_{m,n}} \mathbf{w}_{m,n}^H \mathbf{h}_{m,n} + 1 \\
&= \max_{\omega_{m,n} \geq 0, \beta_{m,n}} \log_2(\omega_{m,n}) - \omega_{m,n} \left(1 - 2\text{Re}\{\beta_{m,n}^* \sqrt{p_{m,n}} \mathbf{w}_{m,n}^H \mathbf{h}_{m,n}\} + |\beta_{m,n}|^2 \left(\sum_{r=1}^{\mathcal{M}} p_{r,n} \left| \mathbf{w}_{m,n}^H \mathbf{h}_{r,n} \right|^2 + \|\mathbf{w}_{m,n}^H\|_2^2 \sigma_{\text{AAV}}^2 \right) \right) + 1 \\
&= \max_{\omega_{m,n} \geq 0, \beta_{m,n}} \tilde{R}_{m,n}.
\end{aligned} \tag{28}$$

$$\tilde{R}_{m,n}^{\text{new}} = \log_2(\omega_{m,n}) - \omega_{m,n} \left(1 - 2\text{Re}\{\beta_{m,n}^* p_{m,n}^{\text{new}} \mathbf{w}_{m,n}^H \mathbf{h}_{m,n}\} + |\beta_{m,n}|^2 \left(\sum_{r=1}^{\mathcal{M}} (p_{r,n}^{\text{new}})^2 \left| \mathbf{w}_{m,n}^H \mathbf{h}_{r,n} \right|^2 + \|\mathbf{w}_{m,n}^H\|_2^2 \sigma_{\text{AAV}}^2 \right) \right) + 1 \tag{36}$$

3) Updating User Transmit Power:

$$(\mathbf{P3-3}) : \max_{\mathbf{P}} \sum_{n=1}^N \sum_{m=1}^M \tilde{R}_{m,n} \tag{34a}$$

$$\text{s.t. (14h).} \tag{34b}$$

By treating $p_{m,n}^{\text{new}} = \sqrt{p_{m,n}}$ as an optimization variable, we obtain a new optimization problem

$$(\mathbf{P3-4}) : \max_{\mathbf{P}^{\text{new}}} \sum_{n=1}^N \sum_{m=1}^M \tilde{R}_{m,n}^{\text{new}} \tag{35a}$$

$$\text{s.t. } 0 \leq p_{m,n}^{\text{new}} \leq \sqrt{P_{\text{max}}}, \forall m \in \mathcal{M}, \forall n \in \mathcal{N}, \tag{35b}$$

where $\mathbf{P}^{\text{new}} \triangleq \{p_{m,n}^{\text{new}}, \forall m, \forall n\}$, and $\tilde{R}_{m,n}^{\text{new}}$ is given in Equation (36).

Problem **(P3-4)** is a convex optimization problem, which can be efficiently solved by standard convex optimization solvers such as CVX. Moreover, by introducing dual variables associated with the constraints (35b), we can derive a Lagrangian dual function and thus an optimal solution can be derived. Concrete information is shown in Theorem 2.

Theorem 2. For problem **(P3-4)**, the optimal user transmit power can be expressed as

$$(p_{m,n}^{\text{new}})^{\text{opt}} = \frac{-\mu_{m,n} + 2\omega_{m,n} \text{Re}\{\beta_{m,n}^* \mathbf{w}_{m,n}^H \mathbf{h}_{m,n}\}}{2 \sum_{r=1}^{\mathcal{M}} \omega_{r,n} |\beta_{r,n}|^2 \left| \mathbf{w}_{r,n}^H \mathbf{h}_{m,n} \right|^2}, \tag{37}$$

where $\{\mu_{m,n}\}$ are the dual variables associated with the corresponding constraints (35b).

Proof. Please refer to Appendix B. \square

The detailed BCA procedure to solve problem **(P3-1)** is summarized in Algorithm 2.

C. Antenna Position of MAs

Given the AAV trajectory \mathbf{Q} , the receive beamforming \mathbf{W} , and the user transmit power \mathbf{P} , the problem can be simplified as the subproblem of optimizing the MA position \mathbf{U} , which is formulated as

$$(\mathbf{P4-1}) : \max_{\mathbf{U}} \sum_{n=1}^N \sum_{m=1}^M R_{m,n} \tag{38a}$$

$$\text{s.t. (14f) – (14g).} \tag{38b}$$

Algorithm 2 BCA-based Algorithm for Solving P3-1

Input: An initial feasible solution \mathbf{W}^0 and \mathbf{P}^0 ;

Initialize: the iteration number $j = 0$;

Initialize: the small precision threshold ϵ ;

Initialize: the maximum number of iterations j_{max} ;

1: **repeat**

2: Update the auxiliary variables and obtain the solution via (30) and (31);

3: Update the receive beamforming by solving **P3-2**;

4: Update the user transmit power by solving **P3-4**;

5: Compute the objective function \tilde{R}^j via (29a);

6: Set $j = j + 1$;

7: **until** $|\tilde{R}^j - \tilde{R}^{j-1}| < \epsilon$ or $j = j_{\text{max}}$;

Output: $\mathbf{W}^j, \mathbf{P}^j, \tilde{R}^j$.

The solutions of \mathbf{U} are independent across different time slots. To reduce the computational complexity, we decompose problem **P4-1** into N subproblems corresponding to different time slots. Hence, each subproblem can be optimized independently. Specifically, the n -th subproblem in time slot n can be formulated as

$$(\mathbf{P4-1.n}) : \max_{\mathbf{U}_n} \sum_{m=1}^M R_{m,n} \tag{39a}$$

$$\text{s.t. } \|\mathbf{u}_{i,n} - \mathbf{u}_{j,n}\| \geq d_{\min}, \forall i \neq j, \forall i, j \in \mathcal{K}, \tag{39b}$$

$$\mathbf{u}_{k,n} \in \mathcal{R}_s, \forall k \in \mathcal{K}, \tag{39c}$$

where \mathbf{U}_n denotes the solution of the antenna position in the n -th time slot. Owing to the strongly non-convex nature of problem **P4-1** and high dimensionality of the solution space of the antenna position, the traditional optimization methods are hard to solve the problem **P4-1**, and incur impractical computational burdens under exhaustive search strategies. Consequently, particle swarm optimization (PSO) is implemented to address this problem [49], [50].

Firstly, we initialize S particles to represent the feasible antenna positions of the MAs. Specifically, the particle set is denoted as $\mathcal{P}_n^{(0)} = \{\mathcal{P}_{1,n}^{(0)}, \mathcal{P}_{2,n}^{(0)}, \dots, \mathcal{P}_{S,n}^{(0)}\}$, where the s -th particle is given by

$$\mathcal{P}_{s,n}^{(0)} = \{\mathbf{u}_{1,n}^{(0)}, \mathbf{u}_{2,n}^{(0)}, \dots, \mathbf{u}_{K,n}^{(0)}\}, \tag{40}$$

where $\mathbf{u}_{k,n}^{(0)} = [x_{k,n}^{(0)}, y_{k,n}^{(0)}] \in \mathcal{R}_s$ denotes the feasible position of the k -th MA. Meanwhile, the velocities of the particles are given by $\mathcal{V}_n^{(0)} = \{\mathcal{V}_{1,n}^{(0)}, \mathcal{V}_{2,n}^{(0)}, \dots, \mathcal{V}_{S,n}^{(0)}\}$.

Let $\tilde{\mathbf{P}}_{s,n}^{\text{L}}$ denote the best position of the s -th particle, and $\tilde{\mathbf{P}}_n^{\text{G}}$ denote the best position of the particle swarm. In each

iteration, the update of the velocity of the s -th particle can be given by

$$\mathbf{v}_{s,n}^{(t+1)} \leftarrow \chi \mathbf{v}_{s,n}^{(t)} + L_1 R_1 \left(\tilde{\mathbf{p}}_{s,n}^L - \mathbf{p}_{s,n}^{(t)} \right) + L_2 R_2 \left(\tilde{\mathbf{p}}_n^G - \mathbf{p}_{s,n}^{(t)} \right), \quad (41)$$

where t denotes the iteration index of the PSO. The individual learning factor L_1 and the global learning factor L_2 determine the step size the particles take toward their individual best position and the swarm's best position, respectively. To increase search randomness and avoid local optima, random variables R_1 and R_2 are sampled uniformly from $[0, 1]$, i.e., $R_1, R_2 \sim \mathcal{U}[0, 1]$. Momentum in particle motion is sustained by the inertia weight χ . Particularly, to balance the trade-off between convergence speed and precision, the inertia weight χ is dynamically decreased during iterations according to

$$\chi = \chi_{\max} - \frac{(\chi_{\max} - \chi_{\min})t}{t_{\max}}, \quad (42)$$

where χ_{\max} and χ_{\min} denote the maximum and minimum value of the inertia weight, respectively. t_{\max} is the maximum iteration number of the PSO. Meanwhile, the position of the s -th particle is update by the velocity, and also constrained by the array region, which can be given by

$$\mathbf{p}_{s,n}^{(t+1)} \leftarrow \min \left(\max \left(\left(\mathbf{p}_{s,n}^{(t)} + \mathbf{v}_{s,n}^{(t+1)} \right), 0 \right), L \right). \quad (43)$$

We evaluate the fitness function as $\bar{\mathcal{R}}(\mathbf{p}_n^{(t)}) = \sum_{n=1}^N \sum_{m=1}^M R_{m,n}(\mathbf{Q}, \mathbf{W}, \mathbf{P})$, for given the trajectory \mathbf{Q} , the receive beamforming \mathbf{W} , and the user transmit power \mathbf{P} . Similarly, we introduce the adaptive penalty factor to the fitness function as

$$F(\mathbf{p}_n^{(t)}) = \bar{\mathcal{R}}(\mathbf{p}_n^{(t)}) - \psi \left| \bar{\mathcal{U}}(\mathbf{p}_n^{(t)}) \right|, \quad (44)$$

where ψ denotes a large positive parameter serves as a penalty factor. $\bar{\mathcal{U}}(\mathbf{p}_n^{(t)})$ denotes the set of the MA position pairs violating the minimum distance constraint in (14f), which can be expressed as

$$\bar{\mathcal{U}}(\mathbf{p}_n^{(t)}) = \{(\mathbf{u}_{i,n}, \mathbf{u}_{j,n}) \mid \|\mathbf{u}_{i,n} - \mathbf{u}_{j,n}\|_2 < d_{\min}, 1 \leq i < j \leq K\}. \quad (45)$$

The penalty factor is introduced to force the particle swarm to exclusively explore the valid positions to ensure the minimum MA distance constraint (39b), as infeasible solutions automatically receive fitness functions (44) below zero. The detailed PSO-based algorithm for addressing problem **P4-1** is summarized in Algorithm 3.

D. Algorithm Analysis

We utilize an AO structure to solve the problem **P1**, and the overall procedure is summarized in Algorithm 4. The following proposition analyze the convergence of Algorithm 4.

Proposition 1. *The objective function of problem **P1** keeps increasing as the number of iterations increases. Therefore, Algorithm 4 is guaranteed to converge.*

Algorithm 3 The PSO-based Algorithm for Solving **P4-1**.

Input: An initial feasible solution \mathbf{U} ;
1: **for** $n = 1$ to N **do**
2: **Initialize:** S particles with initial positions $\mathbf{p}_n^{(0)}$ and velocities $\mathbf{v}_n^{(0)}$, the local best position of each particle, and the global best position of the swarm;
3: Evaluate the initial fitness value;
4: **for** $t = 1$ to t_{\max} **do**
5: Update the inertia weight via (42);
6: **for** $s = 1$ to S **do**
7: Update the velocity of the s -th particle via (41);
8: Update the position of the s -th particle via (43);
9: Calculate the fitness value via (44);
10: **if** $F(\mathbf{p}_{s,n}^{(t)}) > F(\tilde{\mathbf{p}}_{s,n}^L)$ **then**
11: Update $F(\tilde{\mathbf{p}}_{s,n}^L) \leftarrow F(\mathbf{p}_{s,n}^{(t)})$;
12: **end if**
13: **if** $F(\mathbf{p}_{s,n}^{(t)}) > F(\tilde{\mathbf{p}}_n^G)$ **then**
14: Update $F(\tilde{\mathbf{p}}_n^G) \leftarrow F(\mathbf{p}_{s,n}^{(t)})$;
15: **end if**
16: **end for**
17: **end for**
18: **end for**
Output: $\mathbf{U}(\mathbf{p}^{(T)})$ given the position of the swarm $\mathbf{p}_n^{(T)}$, $\forall n \in \mathcal{N}$.

Algorithm 4 AO Algorithm for Solving **P1**

Input: An initial feasible solution \mathbf{Q}^i , \mathbf{W}^i , \mathbf{W}^i , and \mathbf{P}^i ;
Initialize: the iteration number $i = 0$;
Initialize: the small precision threshold ϵ ;
Initialize: the maximum number of iterations i_{\max} ;
1: **repeat**
2: Solving problem **P2-1** via Algorithm 1, get the solution \mathbf{Q}^i ;
3: Solving problem **P3-1** via Algorithm 2, get the solution \mathbf{W}^i and \mathbf{P}^i ;
4: Solving problem **P4-1** via Algorithm 3, get the solution \mathbf{U}^i ;
5: Compute the objective function \bar{R}^i via (14a);
6: Set $i = i + 1$;
7: **until** $|\bar{R}^i - \bar{R}^{i-1}| < \epsilon$ or $i = i_{\max}$;
Output: The optimized solution \mathbf{Q}^i , \mathbf{W}^i , \mathbf{P}^i , and \mathbf{U}^i .

Proof. Please refer to Appendix C. □

In Algorithm 4, we employ the interior-point method to solve the three subproblems: AAV trajectory optimization, user transmit power control, and receive beamforming. The computational complexities of these subproblems are denoted by $\mathcal{O}((2N)^{3.5} \log(\epsilon^{-1}))$, $\mathcal{O}((MN)^{3.5} \log(\epsilon^{-1}))$, and $\mathcal{O}((MNK^2)^{3.5} \log(\epsilon^{-1}))$, respectively, where ϵ represents the stopping tolerance [47], [51]. Furthermore, the PSO algorithm is employed to solve for the MA positions, with a computational complexity denoted by $\mathcal{O}(Nt_{\max}S(2K + \log(S)))$ [49]. Therefore, the total computational complexity of Algorithm 4 is $\mathcal{O}(I_1(\mathcal{O}((2N)^{3.5} \log(\epsilon^{-1}))) + I_2(\mathcal{O}((MN)^{3.5} \log(\epsilon^{-1}))) + \mathcal{O}((MNK^2)^{3.5} \log(\epsilon^{-1}))) + Nt_{\max}S(2K + \log(S)))$, where I_1 denotes the resultant iteration number of Algorithm 4, and I_2 denotes the resultant iteration number of Algorithm 2.

V. NUMERICAL RESULTS

In this section, we provide the numerical results of the proposed scheme with extensive simulation experiments. We consider a square area of 800×800 m² for the data collection mission. The flying height of the AAV is 50 m. To evaluate the performance gain, we compare the proposed schemes with the following three benchmark schemes

- AO-MM Scheme: We utilize the minorization maximization (MM) method to optimize the antenna position, and the detailed procedures are presented in Appendix D.
- Fixed Trajectory Scheme: The trajectory of the AAV is fixed, while the receive beamforming and the antenna position are jointly optimized.
- FPA Scheme: The AAV is equipped with an FPA plane, while the trajectory and the receive beamforming are jointly optimized.

Meanwhile, unless otherwise stated, the default simulation parameters are summarized in Table II.

TABLE II: Simulation Parameters.

Parameters	Value
Mission period, T	40 s
Number of time slot, N	20
Duration of time slot, τ	2 s
Number of user, M	4
Number of antenna, K	4
Number of channel path for each user, L_m^t	4
Carrier wavelength, λ	0.1 m
Size of antenna mobility region, \mathcal{R}_s	$4\lambda \times 4\lambda$
Minimum distance between antennas, d_{\min}	0.5λ
Rician factor, κ	15
Maximum speed, V_{\max}	30 m/s
Maximum acceleration, a_{\max}	10 m/s ²
Maximum transmit power, P_{\max}	1 w
Channel power gain at the reference distance 1m, h_0	-60 dB
Noise power at the AAV, σ_{AAV}	-110 dBm
Number of particles in PSO algorithm, S	100
Maximum iterations in PSO algorithm, t_{\max}	100
Individual learning factor in PSO algorithm, L_1	1.4
Global learning factor in PSO algorithm, L_2	1.4
Minimum inertial weight in PSO algorithm, χ_{\min}	0.4
Maximum inertial weight in PSO algorithm, χ_{\max}	0.9
Penalty factor in PSO algorithm, ψ	20

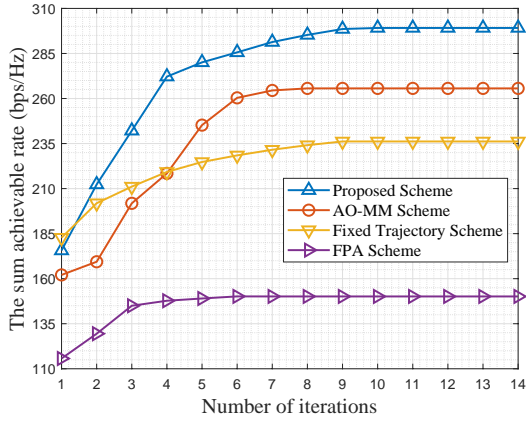


Fig. 2: The convergence performance.

Fig. 2 demonstrates the convergence of the sum achievable rate across different schemes. The proposed scheme achieves over 300 bps/Hz sum achievable rate within 9 iterations, exhibiting the fastest convergence rate among all schemes. Notably, the fixed trajectory scheme exhibits slower convergence and lower sum achievable rate compared to the proposed scheme and the AO-MM scheme, highlighting the vital role of trajectory optimization in overall system performance. Fur-

thermore, the FPA scheme achieves the lowest sum achievable rate at convergence due to its inability to leverage the precise beamforming gains empowered by the MAs.

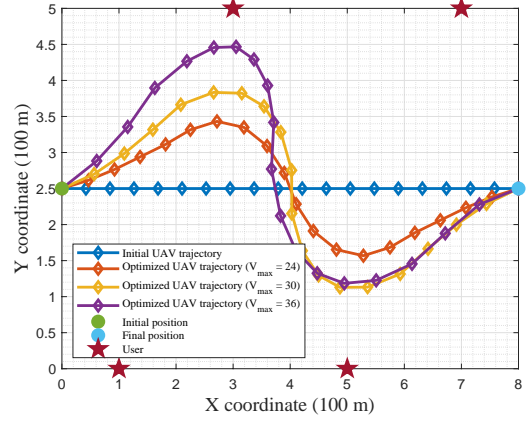


Fig. 3: The optimized trajectory of the AAV.

Fig. 3 presents the optimized trajectories of the AAV under different maximum velocity of the AAV. We can observe that a higher maximum AAV velocity enables the targeted flight trajectory toward the users with better channel conditions, where the MAs leverage precise beamforming to enhance power allocation while suppressing inter-user interference, which is capable of collectively boosting sum achievable rates of users. Conversely, reduced maximum velocity constraints of the AAV prompt balanced trajectory designs ensuring equitable proximity to all users, maintaining optimized spectral efficiency under the AAV mobility limitations.

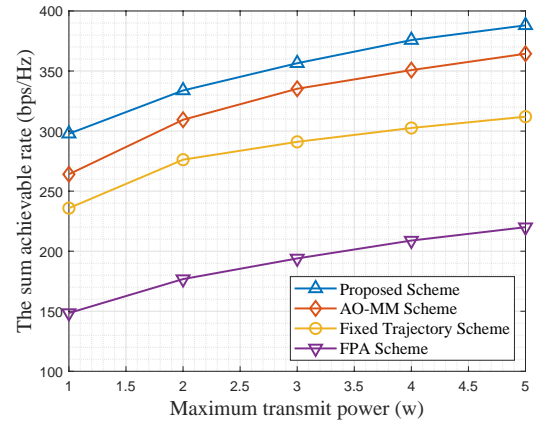


Fig. 4: The sum achievable rate versus maximum transmit power.

Fig. 4 demonstrates that the sum achievable rate for all schemes increases with the maximum transmit power. This is attributed to the enhanced transmit power overcoming the path loss and improving the system SINR. Furthermore, while increasing the maximum transmit power generally improves the sum achievable rate, the marginal gains diminish as the transmit power grows. This saturation effect occurs because higher transmit power, although boosting the desired user's

signal power, proportionally amplify the received interference from other co-channel users. Additionally, the proposed scheme consistently outperforms other schemes. It achieves superior user-oriented beamforming through more effective antenna position optimization, leading to better interference management compared to the AO-MM scheme. In contrast, both the fixed trajectory scheme and the FPA scheme suffer from inefficient beamforming gain, due to their inability to dynamically steer beams optimally towards users, resulting in substantially lower sum achievable rates across the transmit power range.

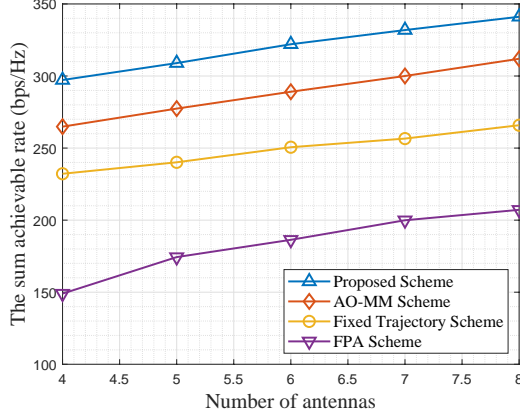


Fig. 5: The sum achievable rate versus number of antennas.

Fig. 5 illustrates the sum achievable rate versus the number of receive antennas at the AAV. We can observe that the increasing number of the receive antennas improves the sum achievable rate for all schemes, primarily due to the enhanced receive beamforming gains and spatial resolution. The proposed scheme demonstrates significant advantage, leveraging its optimized antenna positioning to achieve more precise user-specific beam alignment. This enables superior interference suppression compared to the AO-MM scheme, especially in multi-user scenarios. Conversely, both the fixed trajectory scheme and the FPA scheme exhibit lower sum achievable rate performance. The reason is that, their static configurations cannot dynamically concentrate energy toward specific users, resulting in significantly lower sum achievable rate as the number of receive antennas increases.

Fig. 6 demonstrates that the increasing multi-path components enhance the sum achievable rate across all schemes. This can be attributed to the spatial diversity gain inherent in multi-antenna systems, i.e., the richer scattering environments create additional spatial degrees of freedom, enabling more effective multi-path energy exploitation, and improving the sum achievable rate. The proposed scheme achieves significantly steeper growth by dynamically optimizing antenna positions to coherently combine dominant propagation paths. This adaptive spatial matching maximizes the signal power at target users while suppressing uncorrelated noise. The AO-MM scheme exhibits lower sum achievable rate gains due to the suboptimal antenna positions. The fixed trajectory scheme and the FPA scheme show limited improvements in the sum achievable rate. The reason is that their static configurations cannot exploit

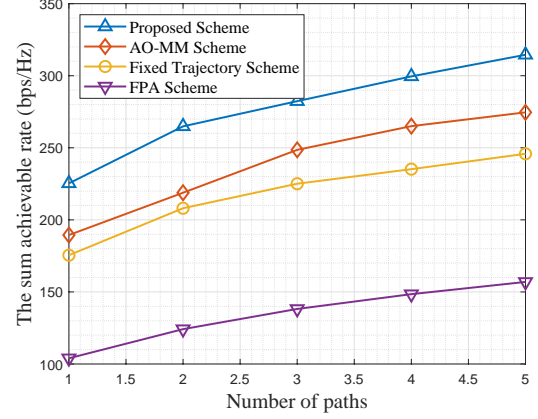


Fig. 6: The sum achievable rate versus number of path.

phase coherence across scattering paths, resulting in lower sum achievable rate compared to the proposed scheme across all paths. This highlights the critical role of dynamic antenna position and AAV maneuver control in harvesting multi-path benefits.

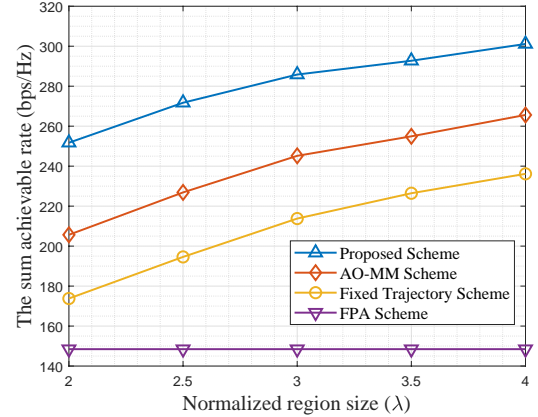


Fig. 7: The sum achievable rate versus the normalized region size.

Fig. 7 shows the sum achievable rate versus the normalized region size. As the normalized region size expands, the sum achievable rate of the schemes with antenna position optimization, i.e., the proposed scheme, the AO-MM scheme, and the fixed trajectory scheme, are increased, while the FPA scheme remains static due to immutable antenna positions. We can observe that the sum achievable rate of the AO-MM scheme is lower than the proposed scheme, which can be attributed to the poorer ability to optimize the antenna position. The fixed trajectory scheme achieves lower sum achievable rate compared to the proposed scheme and the AO-MM scheme since fixed AAV trajectory cannot exploit the mission regions to approach distant users.

Fig. 8 presents the sum achievable rate versus the AAV maximum speed, which reveals a fundamental trade-off between the AAV mobility and communication performance. As the maximum AAV speed increases from 24 m/s to

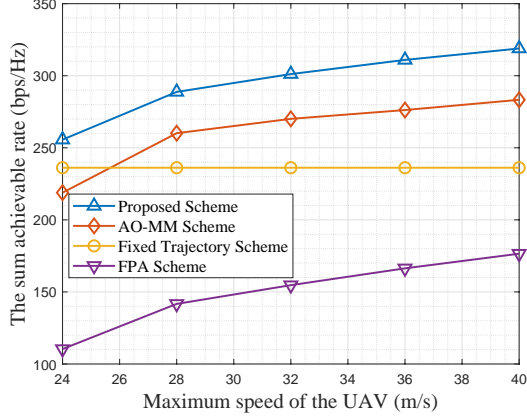


Fig. 8: The sum achievable rate versus the AAV maximum speed.

40 m/s, all trajectory-optimized schemes, i.e., the proposed scheme, the AO-MM scheme, and the FPA scheme, exhibit significant sum achievable rate improvements. The reason is that with increasing maximum speed of the AAV, the propagation distances between the AAV to certain users can be reduced, thus improving the SINR of the certain users. The proposed scheme achieves superior sum achievable rate across all schemes, due to the joint optimization of the AAV trajectory, the antenna positions, and the receive beamforming during movement. Notably, the fixed trajectory scheme shows negligible improvement despite speed increases. The reason is that, its static trajectory fails to exploit mobility for distance reduction, resulting in wasteful energy expenditure without rate benefits. This underscores the necessity of integrated mobility-aware optimization for energy-efficient AAV communication systems.

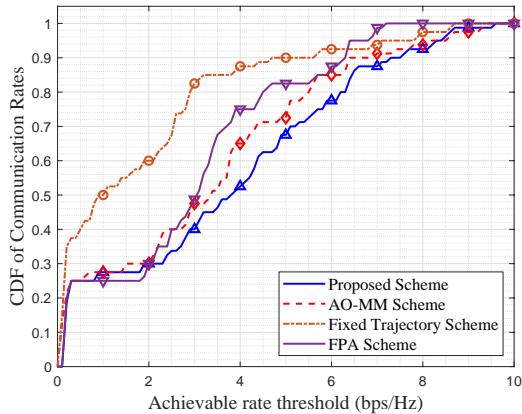


Fig. 9: The CDFs of communication rates versus the achievable rate threshold.

Fig. 9 presents the cumulative distribution functions (CDFs) of communication rates versus the achievable rate threshold, in the perspective of service reliability. We can observe that, 90% of users of the proposed scheme achieves over 7.5 bps/Hz, reflecting robust interference management and consistent chan-

nel quality across the mission period. Most critically, the fixed trajectory scheme and the FPA scheme show severe user QoS degradation, e.g., 30% of users in the fixed trajectory scheme fall below 0.2 bps/Hz due to static trajectory, resulting in beam-user misalignment.

VI. CONCLUSION

In this paper, we investigate an MA-empowered AAV-enabled uplink transmission system, where an AAV is dispatched to collect data from ground users within a designated mission area. We formulate an uplink sum achievable rate maximization problem of all ground users, by jointly optimizing the AAV trajectory, the AAV receive beamforming, and the antenna positions of the MAs. We develop an efficient AO-based algorithm to solve the problem, and analyze the computational complexity and convergence of the proposed scheme to evaluate the executability. The extensive numerical results demonstrate the superior sum achievable rate gains and the service reliability of the proposed scheme compared with several benchmark schemes.

APPENDIX A PROOF OF THEOREM 1

Proof. The Lagrangian function of problem (P3-2) related to receive beamforming can be expressed as

$$\mathcal{L}(\Theta_1) = \sum_{n=1}^N \sum_{m=1}^M \tilde{R}_{m,n} - \sum_{n=1}^N \sum_{m=1}^M \lambda_{m,n} (\|\mathbf{w}_{m,n}\|^2 - 1), \quad (46)$$

where $\Theta_1 = \{\mathbf{w}_{m,n}, \lambda_{m,n}\}$. $\{\lambda_{m,n}, \forall m, \forall n\}$ are the dual variables associated with the corresponding constraints (14e). Thus, the derivations of $\mathcal{L}(\Theta_1)$ with respect to $\mathbf{w}_{m,n}$ can be given by

$$\begin{aligned} \frac{\partial \mathcal{L}(\Theta_1)}{\partial \mathbf{w}_{m,n}} &= -\lambda_{m,n} \mathbf{w}_{m,n}^* + \omega_{m,n} \sqrt{p_{m,n}} \mathbf{h}_{m,n}^* \beta_{m,n} \\ &\quad - \omega_{m,n} |\beta_{m,n}|^2 \left(\sum_{r=1}^M p_{r,n} \mathbf{h}_{m,n}^* \mathbf{h}_{r,n}^T + \sigma_{\text{AAV}}^2 \mathbf{I} \right) \mathbf{w}_{m,n}^*. \end{aligned} \quad (47)$$

By applying the first-order optimality condition, the optimal solution to problem (P3-2) can be obtained by setting the derivatives of $\mathcal{L}(\Theta_1)$ to zero. Thus, the optimal receive beamforming vectors can be given by

$$\begin{aligned} \mathbf{w}_{m,n}^{\text{opt}} &= \frac{\omega_{m,n} \sqrt{p_{m,n}} \mathbf{h}_{m,n} \beta_{m,n}^*}{\omega_{m,n} |\beta_{m,n}|^2 \left(\sum_{r=1}^M p_{r,n} \mathbf{h}_{m,n}^* \mathbf{h}_{r,n}^T + \sigma_{\text{AAV}}^2 \mathbf{I} \right) + \lambda_{m,n} \mathbf{I}}. \end{aligned} \quad (48)$$

□

APPENDIX B PROOF OF THEOREM 2

Proof. The Lagrangian function of problem (P3-3) related to user transmit power control can be expressed as

$$\mathcal{L}(\Theta_2) = \sum_{n=1}^N \sum_{m=1}^M \tilde{R}_{m,n}^{\text{new}} - \sum_{n=1}^N \sum_{m=1}^M \mu_{m,n} \left(p_{m,n}^{\text{new}} - \sqrt{P_{\max}} \right), \quad (49)$$

where $\Theta_2 = \{p_{m,n}^{\text{new}}, \mu_{m,n}\}$. $\{\mu_{m,n}, \forall m, \forall n\}$ are the dual variables associated with the corresponding constraint (35b). Thus, the derivations of $\mathcal{L}(\Theta_2)$ with respect to $p_{m,n}^{\text{new}}$ can be given by

$$\begin{aligned} \frac{\partial \mathcal{L}(\Theta_2)}{\partial p_{m,n}^{\text{new}}} &= -\mu_{m,n} + 2\omega_{m,n} \text{Re}\{\beta_{m,n}^* \mathbf{w}_{m,n}^H \mathbf{h}_{m,n}\} \\ &\quad - \sum_{r=1}^M \omega_{r,n} |\beta_{r,n}|^2 \left(2p_{m,n}^{\text{new}} |\mathbf{w}_{r,n}^H \mathbf{h}_{m,n}|^2 \right). \end{aligned} \quad (50)$$

By applying the first-order optimality condition, the optimal solution to problem (P3-3) can be obtained by setting the derivatives of $\mathcal{L}(\Theta_2)$ to zero. Thus, the optimal receive beamforming vectors can be given by

$$(p_{m,n}^{\text{new}})^{\text{opt}} = \frac{-\mu_{m,n} + 2\omega_{m,n} \text{Re}\{\beta_{m,n}^* \mathbf{w}_{m,n}^H \mathbf{h}_{m,n}\}}{2 \sum_{r=1}^M \omega_{r,n} |\beta_{r,n}|^2 |\mathbf{w}_{r,n}^H \mathbf{h}_{m,n}|^2}. \quad (51)$$

□

APPENDIX C PROOF OF THE PROPOSITION 1

Proof. Let $\mathbf{Q}^i, \mathbf{W}^i, \mathbf{P}^i$, and \mathbf{U}^i denote the solution in the i -th iteration of Algorithm 4, and $\bar{\mathcal{R}}(\mathbf{Q}^i, \mathbf{W}^i, \mathbf{P}^i, \mathbf{U}^i)$ denote the objective function of problem (P1).

Given $\mathbf{W}^i, \mathbf{P}^i$, and \mathbf{U}^i , we solve problem (P2-1) via Algorithm 1 to get the solution \mathbf{Q}^{i+1} . Thus, we have

$$\bar{\mathcal{R}}(\mathbf{Q}^{i+1}, \mathbf{W}^i, \mathbf{P}^i, \mathbf{U}^i) \geq \bar{\mathcal{R}}(\mathbf{Q}^i, \mathbf{W}^i, \mathbf{P}^i, \mathbf{U}^i). \quad (52)$$

Then, given \mathbf{Q}^{i+1} and \mathbf{U}^i , we solve problem (P3-1) via Algorithm 2 to get the AAV receive beamforming \mathbf{W}^{i+1} , and user transmit power \mathbf{P}^{i+1} . Attribute to the BCA, we have

$$\bar{\mathcal{R}}(\mathbf{Q}^{i+1}, \mathbf{W}^{i+1}, \mathbf{P}^{i+1}, \mathbf{U}^i) \geq \bar{\mathcal{R}}(\mathbf{Q}^{i+1}, \mathbf{W}^i, \mathbf{P}^i, \mathbf{U}^i). \quad (53)$$

Then, we solve problem (P4-1) via Algorithm 3 to get the antenna position \mathbf{U}^{i+1} for given $\mathbf{Q}^{i+1}, \mathbf{W}^{i+1}$, and \mathbf{P}^{i+1} . Since the fitness value is non-decreasing, we have

$$\bar{\mathcal{R}}(\mathbf{Q}^{i+1}, \mathbf{W}^{i+1}, \mathbf{P}^{i+1}, \mathbf{U}^{i+1}) \geq \bar{\mathcal{R}}(\mathbf{Q}^{i+1}, \mathbf{W}^{i+1}, \mathbf{P}^{i+1}, \mathbf{U}^i). \quad (54)$$

Combining (52), (53), and (54), we have

$$\bar{\mathcal{R}}(\mathbf{Q}^{i+1}, \mathbf{W}^{i+1}, \mathbf{P}^{i+1}, \mathbf{U}^{i+1}) \geq \bar{\mathcal{R}}(\mathbf{Q}^i, \mathbf{W}^i, \mathbf{P}^i, \mathbf{U}^i), \quad (55)$$

which indicates that the value of the objective function (14a) is non-decreasing over iterations. Moreover, the sum-rate for all users is constrained by the resource constraints on communication, AAV mobility, and energy. Hence, Algorithm 4 is guaranteed to converge. □

APPENDIX D ANTENNA POSITION OPTIMIZATION VIA MM

In this appendix, we present a benchmark scheme based on AO, where the MA positions are optimized via the MM method while other variables follow identical optimization procedures to our proposed scheme.

Specifically, the field response channel matrix $\mathbf{H}_{m,n}$ exhibits a complex and nonlinear relationship with respect to the MA position \mathbf{U} . Accordingly, we transform the problem using the WMMSE method, and the optimization problem can be reformulated as

$$(\mathbf{PD-1}) : \max_{\mathbf{U}, \beta, \omega} \sum_{n=1}^N \sum_{m=1}^M \tilde{R}_{m,n} \quad (56a)$$

$$\text{s.t.} \quad (14f) - (14g), \quad (56b)$$

$$\omega_{m,n} \geq 0, \forall m, \forall n. \quad (56c)$$

Then, we optimize the auxiliary variables based on Eqs. (30) and (31). Similar to pioneer works [52], [53], to reduce computational complexity, we optimize each MA position separately within each time slot, thereby decoupling the relationships between the MAs. Specifically, when optimizing $\{\mathbf{u}_{k,n}, \forall n\}$, all other variables $\{\mathbf{u}_{k',n}, k' \neq k, \forall n\}$ are held fixed. By doing so, the original optimization problem can be decomposed into K separate subproblems, each addressing the optimization of a single MA position.

$$(\mathbf{PD-1.k}) : \max_{\mathbf{u}_{k,n}, \forall n} \sum_{n=1}^N \sum_{m=1}^M \tilde{R}_{m,n} \quad (57a)$$

$$\text{s.t.} \quad \|\mathbf{u}_{k,n} - \mathbf{u}_{k',n}\| \geq d_{\min}, \forall k \neq k', \forall k \in \mathcal{K}, \forall n \in \mathcal{N}, \quad (57b)$$

$$\mathbf{u}_{k,n} \in \mathcal{R}_s, \forall k \in \mathcal{K}, \forall n \in \mathcal{N}. \quad (57c)$$

Regarding $\tilde{R}_{m,n}$, it can be expressed as a function of $\mathbf{u}_{k,n}$, as shown below.

$$\begin{aligned} \tilde{R}_{m,n} &= -\omega_{m,n} |\beta_{m,n}|^2 \sum_{r=1}^M p_{r,n} |\mathbf{w}_{m,n}^H \mathbf{h}_{r,n}|^2 \\ &\quad + 2\omega_{m,n} \text{Re}\{\beta_{m,n}^* \sqrt{p_{m,n}} \mathbf{w}_{m,n}^H \mathbf{h}_{m,n}\} + \Upsilon_{m,n}, \end{aligned} \quad (58)$$

where

$$\Upsilon_{m,n} = \log_2(\omega_{m,n}) - \omega_{m,n} - \omega_{m,n} |\beta_{m,n}|^2 \|\mathbf{w}_{m,n}\|_2^2 \sigma_{\text{AAV}}^2 + 1. \quad (59)$$

For notational convenience, we denote the entry in the i -th row of $\mathbf{w}_{m,n}$ as $w_{m,n,i}$. Then, based on (11), it follows that

$$\begin{aligned} |\mathbf{w}_{m,n}^H \mathbf{h}_{r,n}|^2 &= g_{r,k,n}^H \mathbf{A}_{m,r,k,n} g_{r,k,n} + \text{Re}\{\mathbf{b}_{m,r,k,n}^H g_{r,k,n}\} \\ &\quad + \mathbf{c}_{m,r,k,n}, \end{aligned} \quad (60)$$

$$\text{Re}\{\mathbf{w}_{m,n}^H \mathbf{h}_{m,n}\} = \text{Re}\left\{ \sum_{k=1}^K w_{m,n,k} \mathbf{f}_m^H \Sigma_{m,n}^H g_{m,k,n} \right\}, \quad (61)$$

where

$$\mathbf{A}_{m,r,k,n} = w_{m,n,k} w_{m,n,k}^* \Sigma_{r,n} \mathbf{f}_r \mathbf{f}_r^H \Sigma_{r,n}^H, \quad (62)$$

$$\mathbf{b}_{m,r,k,n} = 2 \sum_{i=1, i \neq k}^K \mathbf{f}_r^H \Sigma_{r,n}^H g_{r,i,n} \Sigma_{r,n} \mathbf{f}_r w_{m,n,i} w_{m,n,k}^*, \quad (63)$$

$$\mathbf{c}_{m,r,k,n} = \left(\sum_{i=1, i \neq k}^K w_{m,n,i} \mathbf{f}_r^H \Sigma_{r,n}^H g_{r,i,n} \right) \times \left(\sum_{j=1, j \neq k}^K w_{m,n,j}^* g_{r,j,n}^H \mathbf{f}_r \Sigma_{r,n} \right). \quad (64)$$

Then, $\tilde{R}_{m,n}$ can be expressed as

$$\tilde{R}_{m,n} = g_{m,k,n}^H \mathbf{E}_{m,k,n} g_{m,k,n} + \text{Re}\{\mathbf{F}_{m,k,n}^H g_{m,k,n}\} + \tilde{\Upsilon}_{m,n}, \quad (65)$$

where

$$\mathbf{E}_{m,k,n} = -\omega_{m,n} |\beta_{m,n}|^2 \sum_{r=1}^M p_{r,n} \mathbf{A}_{m,r,k,n}, \quad (66)$$

$$\mathbf{F}_{m,k,n} = -\omega_{m,n} |\beta_{m,n}|^2 \sum_{r=1}^M p_{r,n} \mathbf{b}_{m,r,k,n} + 2\omega_{m,n} w_{m,n,k} \mathbf{f}_m^H \Sigma_{m,n}^H, \quad (67)$$

$$\begin{aligned} \tilde{\Upsilon}_{m,n} = & \Upsilon_{m,n} + \text{Re}\left\{ \sum_{i=1, i \neq k}^K w_{m,n,i} \mathbf{f}_m^H \Sigma_{m,n}^H g_{m,i,n} \right\} \\ & - \omega_{m,n} |\beta_{m,n}|^2 \sum_{r=1}^M p_{r,n} \mathbf{c}_{m,r,k,n}. \end{aligned} \quad (68)$$

We apply the MM method to tackle the optimization problem [52]. The effectiveness of the MM technique hinges on developing a surrogate function that adheres to the upper bound property for both the objective function and its constraints. In what follows, we present several lemmas that aid in the practical application of the MM method.

Lemma 1. *The quadratic form $\mathbf{x}^H \mathbf{L} \mathbf{x}$, where \mathbf{L} is a Hermitian matrix, can be upper bounded as [52], [54]:*

$$\mathbf{x}^H \mathbf{L} \mathbf{x} \leq \mathbf{x}^H \mathbf{M} \mathbf{x} + 2\text{Re}\{\mathbf{x}^H (\mathbf{L} - \mathbf{M}) \mathbf{x}_0\} + \mathbf{x}_0^H (\mathbf{M} - \mathbf{L}) \mathbf{x}_0, \quad (69)$$

where $\mathbf{M} \succeq \mathbf{L}$. Equality is achieved at $\mathbf{x} = \mathbf{x}_0$.

Lemma 2. $\Psi_{m,n}(\mathbf{u}_{k,n}) = \text{Re}\{\mathbf{\Gamma}^H g_{m,k,n}(\mathbf{u}_{k,n})\}$ can be bounded from both below and above as follows [53]

$$\begin{aligned} \Psi_{m,n}(\mathbf{u}_{k,n}) \geq & \Psi_{m,n}(\mathbf{u}_{k,n}^{(l)}) + \nabla \Psi_{m,n}(\mathbf{u}_{k,n}^{(l)})^T (\mathbf{u}_{k,n} - \mathbf{u}_{k,n}^{(l)}) \\ & - \frac{4\pi^2}{\lambda^2} \|\mathbf{\Gamma}\|_1 (\mathbf{u}_{k,n} - \mathbf{u}_{k,n}^{(l)})^T (\mathbf{u}_{k,n} - \mathbf{u}_{k,n}^{(l)}), \end{aligned} \quad (70)$$

$$\begin{aligned} \Psi_{m,n}(\mathbf{u}_{k,n}) \leq & \Psi_{m,n}(\mathbf{u}_{k,n}^{(l)}) + \nabla \Psi_{m,n}(\mathbf{u}_{k,n}^{(l)})^T (\mathbf{u}_{k,n} - \mathbf{u}_{k,n}^{(l)}) \\ & + \frac{4\pi^2}{\lambda^2} \|\mathbf{\Gamma}\|_1 (\mathbf{u}_{k,n} - \mathbf{u}_{k,n}^{(l)})^T (\mathbf{u}_{k,n} - \mathbf{u}_{k,n}^{(l)}), \end{aligned} \quad (71)$$

where

$$\nabla \Psi_{m,n}(\mathbf{u}_{k,n}^{(l)}) = \text{Re}\{\mathbf{\Gamma}^H \nabla g_{m,k,n}^{(l)}\}^T, \quad (72)$$

$$\nabla g_{m,k,n}^{(l)} = j \frac{2\pi}{\lambda} (\mathbf{n}_{m,1,n}, \dots, \mathbf{n}_{m,L_m,n})^T \odot (g_{m,k,n}^{(l)}, g_{m,k,n}^{(l)}), \quad (73)$$

$$\mathbf{n}_{m,i,n} = (\sin \theta_{m,i,n} \cos \phi_{m,i,n}, \sin \theta_{m,i,n} \sin \phi_{m,i,n})^T, \quad (74)$$

where we denote $g_{m,k,n}(\mathbf{u}_{k,n}^{(l)})$ as $g_{m,k,n}^{(l)}$ for notational convenience. The equality is achieved at $\mathbf{u}_{k,n} = \mathbf{u}_{k,n}^{(l)}$.

Based on Lemmas 1 and 2, a minorizing function for the objective function can be expressed by (75) at the l -th iteration and evaluated at $\mathbf{u}_{k,n} = \mathbf{u}_{k,n}^{(l)}$, where $\mathbf{\Gamma} = \mathbf{J}_{m,k,n}$, and

$$\zeta_{m,k,n} = -\omega_{m,n} |\beta_{m,n}|^2 \sum_{r=1}^M p_{r,n} w_{m,n,k} w_{m,n,k}^* \|\Sigma_{r,n} \mathbf{f}_r\|^2. \quad (76)$$

Based on the Cauchy-Schwarz inequality, a minorizing function for the constraint is developed at $\mathbf{u}_{k,n} = \mathbf{u}_{k,n}^{(l)}$ during the l -th iteration, as described below

$$\|\mathbf{u}_{k,n} - \mathbf{u}_{k',n}\|_2 \geq \frac{(\mathbf{u}_{k,n}^{(l)} - \mathbf{u}_{k',n})^T (\mathbf{u}_{k,n} - \mathbf{u}_{k',n})}{\|\mathbf{u}_{k,n}^{(l)} - \mathbf{u}_{k',n}\|_2}. \quad (77)$$

In the end, the MA position optimization problem can be expressed as

$$(\text{PD-2.k}) : \max_{\mathbf{u}_{k,n}, \forall n} \sum_{n=1}^N \sum_{m=1}^M \tilde{R}_{m,n}^{\text{new}} \quad (78a)$$

$$\text{s.t.} \quad (57c), (77). \quad (78b)$$

This is a typical convex quadratic programming (QP) problem and can be efficiently solved using quadprog or CVX.

REFERENCES

- [1] G. Cheng, X. Song, Z. Lyu, and J. Xu, "Networked ISAC for low-altitude economy: Coordinated transmit beamforming and UAV trajectory design," *IEEE Trans. Commun.*, to appear, 2025.
- [2] Z. Kuang, W. Liu, C. Wang, Z. Jin, J. Ren, X. Zhang, and Y. Shen, "Movable-antenna array empowered ISAC systems for low-altitude economy," in *Proc. IEEE/CIC Int. Conf. Commun. China Workshops (ICCC Workshops)*, Hangzhou, China, Aug. 2024, pp. 776–781.
- [3] Q. Wu, J. Xu, Y. Zeng, D. W. K. Ng, N. Al-Dhahir, R. Schober, and A. L. Swindlehurst, "A comprehensive overview on 5G-and-beyond networks with UAVs: From communications to sensing and intelligence," *IEEE J. Sel. Areas Commun.*, vol. 39, no. 10, pp. 2912–2945, Oct. 2021.
- [4] Y. Zeng, Q. Wu, and R. Zhang, "Accessing from the sky: A tutorial on UAV communications for 5G and beyond," *Proc. IEEE*, vol. 107, no. 12, pp. 2327–2375, Dec. 2019.
- [5] W. Liu, H. Wang, X. Zhang, H. Xing, J. Ren, Y. Shen, and S. Cui, "Joint trajectory design and resource allocation in UAV-enabled heterogeneous MEC systems," *IEEE Internet Things J.*, vol. 11, no. 19, pp. 30817–30832, Oct. 2024.
- [6] M. Shafi, A. F. Molisch, P. J. Smith, T. Haustein, P. Zhu, P. De Silva, F. Tufvesson, A. Benjebbour, and G. Wunder, "5G: A tutorial overview of standards, trials, challenges, deployment, and practice," *IEEE J. Sel. Areas Commun.*, vol. 35, no. 6, pp. 1201–1221, Jun. 2017.
- [7] A. F. Molisch, V. V. Ratnam, S. Han, Z. Li, S. L. H. Nguyen, L. Li, and K. Haneda, "Hybrid beamforming for massive MIMO: A survey," *IEEE Commun. Mag.*, vol. 55, no. 9, pp. 134–141, Sep. 2017.
- [8] W. Feng, J. Tang, N. Zhao, X. Zhang, X. Wang, K.-K. Wong, and J. A. Chambers, "Hybrid beamforming design and resource allocation for UAV-aided wireless-powered mobile edge computing networks with NOMA," *IEEE J. Sel. Areas Commun.*, vol. 39, no. 11, pp. 3271–3286, Nov. 2021.
- [9] Z. Li, J. Ba, Z. Su, J. Huang, H. Peng, W. Chen, L. Du, and T. H. Luan, "Movable antennas enabled ISAC systems: Fundamentals, opportunities, and future directions," *IEEE Wireless Commun.*, to appear, 2025.
- [10] L. Zhu and K.-K. Wong, "Historical review of fluid antenna and movable antenna," *arXiv preprint arXiv:2401.02362*, 2024.
- [11] L. Zhu, W. Ma, and R. Zhang, "Movable antennas for wireless communication: Opportunities and challenges," *IEEE Commun. Mag.*, vol. 62, no. 6, pp. 114–120, Jun. 2024.
- [12] W. Liu, X. Zhang, C. Wang, J. Ren, and W. Yuan, "Movable antennas meet low-altitude wireless networks: Fundamentals, opportunities, and future directions," *arXiv preprint arXiv:2506.13250*, 2025.

$$\begin{aligned}
\tilde{R}_{m,n} &= g_{m,k,n}^H \mathbf{E}_{m,k,n} g_{m,k,n} + \text{Re}\{\mathbf{F}_{m,k,n}^H g_{m,k,n}\} + \tilde{\Upsilon}_{m,n} \\
&\geq \zeta_{m,k,n} g_{m,k,n}^H \mathbf{I} g_{m,k,n} + 2\text{Re}\{g_{m,k,n}^H (\mathbf{E}_{m,k,n} - \zeta_{m,k,n} \mathbf{I}) g_{m,k,n}^{(l)}\} + (g_{m,k,n}^{(l)})^H (\zeta_{m,k,n} \mathbf{I} - \mathbf{E}_{m,k,n}) g_{m,k,n}^{(l)} \\
&\quad + \text{Re}\{\mathbf{F}_{m,k,n}^H g_{m,k,n}\} + \tilde{\Upsilon}_{m,n} \\
&= \text{Re}\{\underbrace{((2\mathbf{E}_{m,k,n} g_{m,k,n}^{(l)} - 2\zeta_{m,k,n} \mathbf{I} g_{m,k,n}^{(l)})^H + \mathbf{F}_{m,k,n}^H) g_{m,k,n}}_{\mathbf{J}_{m,k,n}^H}\} + (g_{m,k,n}^{(l)})^H (\zeta_{m,k,n} \mathbf{I} - \mathbf{E}_{m,k,n}) g_{m,k,n}^{(l)} + \tilde{\Upsilon}_{m,n} \quad (75) \\
&\geq \text{Re}\{\mathbf{J}_{m,k,n}^H g_{m,k,n}^{(l)}\} \Psi_{m,n}(\mathbf{u}_{k,n}^{(l)}) + \nabla \Psi_{m,n}(\mathbf{u}_{k,n}^{(l)})^T (\mathbf{u}_{k,n} - \mathbf{u}_{k,n}^{(l)}) + \frac{4\pi^2}{\lambda^2} \|\mathbf{J}_{m,k,n}\|_1 (\mathbf{u}_{k,n} - \mathbf{u}_{k,n}^{(l)})^T (\mathbf{u}_{k,n} - \mathbf{u}_{k,n}^{(l)}) \\
&= \tilde{R}_{m,n}^{\text{new}},
\end{aligned}$$

-
- [13] L. Zhu, W. Ma, and R. Zhang, "Modeling and performance analysis for movable antenna enabled wireless communications," *IEEE Trans. Wireless Commun.*, vol. 23, no. 6, pp. 6234–6250, Jun. 2024.
- [14] C. Dou, Y. Wu, L. Qian, K.-K. Wong, and T. Q. S. Quek, "Fluid antenna empowered integration of sensing, communications and computing with hybrid multi-task offloading," *IEEE Wireless Commun. Lett.*, to appear, 2025.
- [15] Y. Bai, B. Xie, R. Zhu, Z. Chang, and R. Jantti, "Movable antenna-equipped UAV for data collection in backscatter sensor networks: A deep reinforcement learning-based approach," *arXiv preprint arXiv:2411.13970*, 2024.
- [16] J. Cui, Y. Liu, and A. Nallanathan, "Multi-agent reinforcement learning-based resource allocation for UAV networks," *IEEE Trans. Wireless Commun.*, vol. 19, no. 2, pp. 729–743, Feb. 2020.
- [17] C. H. Liu, X. Ma, X. Gao, and J. Tang, "Distributed energy-efficient multi-UAV navigation for long-term communication coverage by deep reinforcement learning," *IEEE Trans. Mobile Comput.*, vol. 19, no. 6, pp. 1274–1285, Jun. 2020.
- [18] F. Cheng, G. Gui, N. Zhao, Y. Chen, J. Tang, and H. Sari, "UAV-relaying-assisted secure transmission with caching," *IEEE Trans. Commun.*, vol. 67, no. 5, pp. 3140–3153, May 2019.
- [19] A. Ranjha and G. Kaddoum, "URLLC facilitated by mobile UAV relay and RIS: A joint design of passive beamforming, blocklength, and UAV positioning," *IEEE Internet Things J.*, vol. 8, no. 6, pp. 4618–4627, Mar. 2021.
- [20] W. Luo, Y. Shen, B. Yang, S. Wang, and X. Guan, "Joint 3-D trajectory and resource optimization in multi-UAV-enabled IoT networks with wireless power transfer," *IEEE Internet Things J.*, vol. 8, no. 10, pp. 7833–7848, May 2021.
- [21] S. Gong, M. Wang, B. Gu, W. Zhang, D. T. Hoang, and D. Niyato, "Bayesian optimization enhanced deep reinforcement learning for trajectory planning and network formation in multi-UAV networks," *IEEE Trans. Veh. Technol.*, vol. 72, no. 8, pp. 10933–10948, Aug. 2023.
- [22] Z. Lyu, G. Zhu, and J. Xu, "Joint maneuver and beamforming design for UAV-enabled integrated sensing and communication," *IEEE Trans. Wireless Commun.*, vol. 22, no. 4, pp. 2424–2440, Apr. 2023.
- [23] W. Liu, Z. Jin, X. Zhang, W. Zang, S. Wang, and Y. Shen, "AoI-aware UAV-enabled marine MEC networks with integrated sensing, computation, and communication," in *Proc. IEEE/CIC Int. Conf. Commun. China Workshops (ICCC Workshops)*, Dalian, China, Aug. 2023, pp. 1–6.
- [24] S. Bi, J. Yu, Z. Yang, X. Lin, and Y. Wu, "Joint 3-D deployment and resource allocation for UAV-assisted integrated communication and localization," *IEEE Wireless Commun. Lett.*, vol. 12, no. 10, pp. 1672–1676, Oct. 2023.
- [25] T. V. Nguyen, H. D. Le, and A. T. Pham, "On the design of RIS-UAV relay-assisted hybrid FSO/RF satellite-aerial-ground integrated network," *IEEE Trans. Aerosp. Electron. Syst.*, vol. 59, no. 2, pp. 757–771, Apr. 2023.
- [26] Q. Xu, Z. Su, D. Fang, and Y. Wu, "Hierarchical bandwidth allocation for social community-oriented multicast in space-air-ground integrated networks," *IEEE Trans. Wireless Commun.*, vol. 22, no. 3, pp. 1915–1930, Mar. 2023.
- [27] W. Liu, J. Wang, H. Xing, Z. Jin, X. Zhang, and Y. Shen, "Blockchain-empowered space-air-ground integrated networks for remote internet of things," in *Proc. IEEE/CIC Int. Conf. Commun. China*, Dalian, China, Aug. 2023, pp. 1–6.
- [28] X. Chen, Z. Chang, M. Liu, N. Zhao, T. Hämmäläinen, and D. Niyato, "UAV-IRS assisted covert communication: Introducing uncertainty via phase shifting," *IEEE Wireless Commun. Lett.*, vol. 13, no. 1, pp. 103–107, Jan. 2024.
- [29] L. P. Qian, W. Zhang, Q. Wang, Y. Wu, and X. Yang, "Alternative optimization for secrecy throughput maximization in UAV-aided NOMA networks," *IEEE Wireless Commun. Lett.*, vol. 11, no. 12, pp. 2580–2584, Dec. 2022.
- [30] X. Zhang, W. Luo, Y. Shen, and S. Wang, "Average AoI minimization in UAV-assisted IoT backscatter communication systems with updated information," in *Proc. IEEE Ubiquitous Intell. Comput. (UIC)*, Atlanta, GA, USA, Oct. 2021, pp. 123–130.
- [31] Y. Long, S. Zhao, S. Gong, B. Gu, D. Niyato, and X. Shen, "AoI-aware sensing scheduling and trajectory optimization for multi-UAV-assisted wireless backscatter networks," *IEEE Trans. Veh. Technol.*, vol. 73, no. 10, pp. 15440–15455, Oct. 2024.
- [32] Z. Wei, M. Zhu, N. Zhang, L. Wang, Y. Zou, Z. Meng, H. Wu, and Z. Feng, "UAV-assisted data collection for internet of things: A survey," *IEEE Internet Things J.*, vol. 9, no. 17, pp. 15460–15483, Sep. 2022.
- [33] X. Zhang, H. Xing, Y. Shen, J. Xu, and S. Cui, "Age of information minimization in UAV-enabled IoT networks via federated reinforcement learning," *IEEE Trans. Wireless Commun.*, to appear, 2025.
- [34] S. Fu, Y. Tang, Y. Wu, N. Zhang, H. Gu, C. Chen, and M. Liu, "Energy-efficient UAV-enabled data collection via wireless charging: A reinforcement learning approach," *IEEE Internet Things J.*, vol. 8, no. 12, pp. 10209–10219, Jun. 2021.
- [35] Z. Yu, Y. Gong, S. Gong, and Y. Guo, "Joint task offloading and resource allocation in UAV-enabled mobile edge computing," *IEEE Internet Things J.*, vol. 7, no. 4, pp. 3147–3159, Apr. 2020.
- [36] M. Dai, Z. Luo, Y. Wu, L. Qian, B. Lin, and Z. Su, "Incentive oriented two-tier task offloading scheme in marine edge computing networks: A hybrid stackelberg-auction game approach," *IEEE Trans. Wireless Commun.*, vol. 22, no. 12, pp. 8603–8619, Dec. 2023.
- [37] M. Fu, Y. Zhou, Y. Shi, C. Jiang, and W. Zhang, "UAV-assisted multi-cluster over-the-air computation," *IEEE Trans. Wireless Commun.*, vol. 22, no. 7, pp. 4668–4682, Jul. 2023.
- [38] Y. Chen, S. Sun, M. Liu, B. Ai, Y. Wang, and Y. Liu, "Energy-efficient over-the-air computation in UAV-assisted IIoT networks," *IEEE Trans. Mobile Comput.*, to appear, 2025.
- [39] M. Fu, Y. Shi, and Y. Zhou, "Federated learning via unmanned aerial vehicle," *IEEE Trans. Wireless Commun.*, vol. 23, no. 4, pp. 2884–2900, Apr. 2024.
- [40] Z. Zhai, X. Yuan, X. Wang, and H. Yang, "UAV-enabled asynchronous federated learning," *IEEE Trans. Wireless Commun.*, vol. 24, no. 3, pp. 2358–2372, Mar. 2025.
- [41] X. Zhang, W. Liu, J. Ren, H. Xing, G. Gui, Y. Shen, and S. Cui, "Latency minimization for UAV-enabled federated learning: Trajectory design and resource allocation," *IEEE Internet Things J.*, vol. 12, no. 14, pp. 27097–27112, Jul. 2025.
- [42] W. Liu, X. Zhang, H. Xing, J. Ren, Y. Shen, and S. Cui, "UAV-enabled wireless networks with movable-antenna array: Flexible beamforming and trajectory design," *IEEE Wireless Commun. Lett.*, vol. 14, no. 3, pp. 566–570, Mar. 2025.
- [43] T. Ren, X. Zhang, L. Zhu, W. Ma, X. Gao, and R. Zhang, "6D movable antenna enhanced interference mitigation for cellular-connected UAV communications," *IEEE Wireless Commun. Lett.*, vol. 14, no. 6, pp. 1618–1622, Jun. 2025.
- [44] D. Xu, Y. Sun, D. W. K. Ng, and R. Schober, "Multiuser MISO UAV communications in uncertain environments with no-fly zones: Robust trajectory and resource allocation design," *IEEE Trans. Commun.*, vol. 68, no. 5, pp. 3153–3172, May 2020.
- [45] H. Qin, W. Chen, Z. Li, Q. Wu, N. Cheng, and F. Chen, "Antenna positioning and beamforming design for fluid antenna-assisted multi-user downlink communications," *IEEE Wireless Commun. Lett.*, vol. 13, no. 4, pp. 1073–1077, Apr. 2024.
- [46] A. Khalili and R. Schober, "Advanced ISAC design: Movable antennas and accounting for dynamic RCS," in *Proc. IEEE Glob. Commun. Conf. (GLOBECOM)*, Cape Town, South Africa, Dec. 2024, pp. 4022–4027.

- [47] C. Deng, X. Fang, and X. Wang, "Beamforming design and trajectory optimization for UAV-empowered adaptable integrated sensing and communication," *IEEE Trans. Wireless Commun.*, vol. 22, no. 11, pp. 8512–8526, Nov. 2023.
- [48] Q. Shi, M. Razaviyayn, Z.-Q. Luo, and C. He, "An iteratively weighted MMSE approach to distributed sum-utility maximization for a MIMO interfering broadcast channel," *IEEE Trans. Signal Process.*, vol. 59, no. 9, pp. 4331–4340, Sep. 2011.
- [49] Z. Xiao, X. Pi, L. Zhu, X.-G. Xia, and R. Zhang, "Multiuser communications with movable-antenna base station: Joint antenna positioning, receive combining, and power control," *IEEE Trans. Wireless Commun.*, vol. 23, no. 12, pp. 19 744–19 759, Dec. 2024.
- [50] J. Ding, Z. Zhou, and B. Jiao, "Movable antenna-aided secure full-duplex multi-user communications," *IEEE Trans. Wireless Commun.*, vol. 24, no. 3, pp. 2389–2403, Mar. 2025.
- [51] Z.-q. Luo, W.-k. Ma, A. M.-c. So, Y. Ye, and S. Zhang, "Semidefinite relaxation of quadratic optimization problems," *IEEE Signal Processing Magazine*, vol. 27, no. 3, pp. 20–34, May 2010.
- [52] B. Feng, Y. Wu, X.-G. Xia, and C. Xiao, "Weighted sum-rate maximization for movable antenna-enhanced wireless networks," *IEEE Wireless Commun. Lett.*, vol. 13, no. 6, pp. 1770–1774, Jun. 2024.
- [53] W. Ma, L. Zhu, and R. Zhang, "MIMO capacity characterization for movable antenna systems," *IEEE Trans. Wireless Commun.*, vol. 23, no. 4, pp. 3392–3407, Apr. 2024.
- [54] Y. Sun, P. Babu, and D. P. Palomar, "Majorization-minimization algorithms in signal processing, communications, and machine learning," *IEEE Trans. Signal Process.*, vol. 65, no. 3, pp. 794–816, Feb. 2016.